UNIVERSITY OF THESSALY
SCHOOL OF ENGINEERING
DEPARTMENT OF MECHANICAL ENGINEERING

Master Thesis

Incremental Homogenization Estimates for Particulate Composites

by

ATHANASIOS PATSIOURAS

Diploma in Mechanical Engineering, University of Thessaly, 2015

A Thesis
Submitted in Partial Fulfillment of the
Requirements for the Degree of
Master of Science
2018

Approved by the Three Members of the Advisor Committee

First Member (Supervisor)	Michalis Agoras Assistant Professor, Department of Mechanical Engineering University of Thessaly
Second Member	Nikolaos Aravas Professor, Department of Mechanical Engineering University of Thessaly
Third Member	Alexis Kermanidis Assistant Professor, Department of Mechanical Engineering University of Thessaly

Ευχαριστίες

Πρώτα απ΄ όλα, θέλω να ευχαριστήσω τον επιβλέποντα της εργασίας μου, Επίκουρο Καθηγητή κ. Μιχάλη Αγόρα, για την καθοδήγηση και την πολύτιμη βοήθεια που μου προσέφερε κατά τη διάρκεια της δουλειάς μου. Επίσης, θα ήθελα να ευχαριστήσω τα μέλη της εξεταστικής επιτροπής της εργασίας μου, Καθηγητή κ. Νικόλαο Αράβα και Επίκουρο Καθηγητή κ. Αλέξη Κερμανίδη για το χρόνο που διέθεσαν για την ανάγνωση και αξιολόγηση της εργασίας.

Ευχαριστώ ιδιαίτερα τη Λευκή για την υποστήριξη που μου παρείχε καθώς και την κατανόση που έδειξε όλο αυτό το διάστημα.

Τέλος, θα ήθελα να ευχαριστήσω τους γονείς μου και την αδερφή μου για τη συνεχή και αμέριστη υποστήριξη τους καθ΄ όλη τη διάρκεια των σπουδών μου.

Πατσιούρας Αθανάσιος

Contents

List of Figures

Chapter 1

Introduction

A composite material is a heterogeneous medium consisting of two or more homogeneous materials (phases) with different properties that are distributed at a length scale much smaller than the length scale of the overall dimensions of the composite. Many natural and artificial materials are of this nature such as: glass fiber reinforced plastics, ceramic particle reinforced metal matrix composites, polycrystalline metals,etc.

Homogenization methods aim to determine the "effective" or "average" properties of composites directly from the properties of the constitutive phases and their arrangement within the composite. For linear elastic composites there are available many methods for estimating their effective behavior. Simple estimates for the effective elastic moduli of composites and polycrystals were derived by Voigt and Reuss, who assumed uniform strain and uniform stress, respectively. Bishop and Hill (1952) [4, 5], by means of the principles of minimum potential and complementary energy, have shown that these results are upper and lower bounds, respectively. Decades later, Eshelby gave the exact solution to the problem of an ellipsoidal elastic inclusion embedded in an infinite uniform elastic matrix under arbitrary uniform boundary condition (Eshelby, 1957 [6]). Eshelby's solution can be easily extended to determine the effective behavior of dilute composites. In addition, an exact result has been introduced by Hashin [8] for the effective bulk modulus of a special class of microstructures called the composite spheres assemblage (CSA). Later, Hashin and Shtrikman (HS) [9] developed a variational principle that yields bounds for composites with statistically isotropic phase geometry. These bounds are significant improvement to the Voigt-Reuss bounds. It is important to mention that one-point and two-point statistics for the phase distribution are used in the HS bounds. Further contribution made from Willis [27], who generalized the Hashin and Shtrikman bounds for composites with a more general ellipsoidal symmetry for the two-point probabilities. For particulate material systems, more specific estimates have been given by Ponte Castañeda and Willis [18] still using the variational method of HS. In addition to the above mentioned methods, many approximations for estimating effective moduli of composites a have been introduced. A well-known approximation for effective properties of particulate composites is the differential scheme (DS), introduced by Bruggeman [3] in the context of conductivity.

For nonlinear composites, first improvement to Voigt and Reuss bounds have been given from Talbot and Willis [26], who generalized the Hashin and Strickman variational

principle for nonlinear composites materials. A more general variational method proposed later from Ponte Castañeda [19, 20] that allow the derivation of a more general class of bounds and estimates. This method predicts the effective properties of a nonlinear composite by means of an optimal chosen linear comparison composite (LCC). Most recently, a new symmetric fully optimized second order method (FOSO) was introduced by Ponte Castañeda and Furer [7], building on previous second order methods of Ponte Castañeda [21, 23]. This method is known to yield the most accurate estimates to date for nonlinear materials.

Previous works of Agoras and Ponte Castañeda [1, 2] has shown that improved estimates for nonlinear composites may be obtained by utilizing iterated homogenization. Motivated by this finding, in this thesis, following Agoras and Ponte Castañeda [1] we will use a sequential homogenization procedure for estimating the effective behavior of composite materials. However, unlike the recent work of Agoras and Ponte Castañeda [2] where the matrix phase was added incrementally, starting with high volume fractions of inclusions, we will use a discretized version of the DS where the composite is constructed by the gradual addition of small amounts of inclusions to a homogeneous matrix material. Thus, the estimates that will be obtained in this work are expected to be different in general than the corresponding estimates of Agoras and Ponte Castañeda [2].

This thesis is laid out as follows. Chapter 2, introduces the homogenization framework that this work is based on. The necessary background will be presented, including the definition of the microstructure, the local constitutive behavior of the phases and a general variational formulation for the homogenization problem. Next, we will discuss the constitutive relations that can be obtained in the context of linear elastic materials. Chapter 3, deals with the determination of the effective behavior of linear and nonlinear elastic, two-phase, particulate composites. First, we will present the Ponte Castañeda-Willis [18] (PCW) estimates for the effective modulus tensors of linear elastic particulate composites. In the sequel, we provide a brief description of the variational method of Ponte Castañeda for the determination of the effective behavior of nonlinear composites. In Chapter 4 we will describe the "incremental homogenization" (IH) scheme that we will use for estimating the effective behavior of both linear and nonlinear composites. Finally, in Chapter 5 we will present several applications of the incremental homogenization within the context of linear and nonlinear composites, including rigidly reinforced composites, porous materials and two phase composites with specific heterogeneity contrast.

In this work, scalars will be denoted by italic Roman, a, or Greek letters, α; vectors by boldface Roman letters, $\mathbf{P}$; second-order tensors by boldface italic Roman letters, $\boldsymbol{Z}$, or Greek letters, $\boldsymbol{\sigma}$; and fourth-order tensors by barred letters, $\mathbb{C}$. When necessary, Cartesian components will be introduced, such that, for example, $P_i, \sigma_{ij}, C_{ijkl}$ are the Cartesian components of $\mathbf{P}$, $\boldsymbol{\sigma}$, and $\mathbb{C}$, respectively. The summation notation is used for repeated indices. Dyadic (or tensor) products will be denoted by the symbol $\otimes$ (e.g $(\mathbf{u} \otimes \mathbf{v})_{ij} = u_i v_j$ and $(\boldsymbol{\sigma} \otimes \boldsymbol{\sigma})_{ijkl} = \sigma_{ij}\sigma_{kl}$) and the various other products by dots (e.g. $\mathbf{u} \cdot \mathbf{v} = u_i v_i, (\mathbb{C} : \boldsymbol{\epsilon})_{ij} = \mathbb{C}_{ijkl}\epsilon_{kl}$).

Chapter 2

Background

2.1 Prelimaries

We consider a "representative volume element" (RVE) of a 2-phase composite material made up of a family of inclusions (phase 2) that are distributed randomly over a matrix material (phase 1), as shown in Fig. 2.1 The volume of the RVE is denoted as Ω and the sub-regions of the RVE occupied by each phase r as $\Omega^{(r)}$, with $r = 1, 2$. The notations $\langle\cdot\rangle$ and $\langle\cdot\rangle^{(r)}$ will be used in this work to denote the volume average of a field over Ω and $\Omega^{(r)}$, respectively. We make the assumption that the size of the inclusions ℓ is much smaller than the characteristic lenght scale L of the RVE

$$\ell << L. \tag{2.1}$$

The distribution of the constituent phases in the RVE Ω is described by means of characteristic functions $\chi^{(r)}(\mathbf{x})$ as follows

$$\chi^{(r)}(\mathbf{x}) = \begin{cases} 1, & \mathbf{x} \in \Omega^{(r)} \\ 0, & otherwise \end{cases}. \tag{2.2}$$

Hence, the corresponding volume fractions $c^{(r)}$ of the matrix and inclusion phases may be written in terms of the associated characteristic functions as $c^{(r)} \equiv |\Omega^{(r)}|/|\Omega| = \langle\chi^{(r)}(\mathbf{x})\rangle$. Furthermore, we assume that the microstructures of interest are statistically uniform, ergodic and possesses no long -range order (see e.g. Willis, 1981 [28]).

The constitutive behavior of the phases is assumed to be characterized by the stress potentials $u^{(r)}(\boldsymbol{\sigma})$, which are taken to be *convex* functions of the Cauchy stress tensor $\boldsymbol{\sigma}$. In this case, the local constitutive relation between the strain tensor $\boldsymbol{\epsilon}$ and the stress tensor $\boldsymbol{\sigma}$ is given by

$$\boldsymbol{\epsilon} = \frac{\partial u}{\partial \boldsymbol{\sigma}}(\mathbf{x}, \boldsymbol{\sigma}), \tag{2.3}$$

where

$$u(\mathbf{x}, \boldsymbol{\sigma}) = \sum_{r=1}^{N} \chi^{(r)}(\mathbf{x})\ u^{(r)}(\boldsymbol{\sigma}) \tag{2.4}$$

is the local stress potential of the composite.

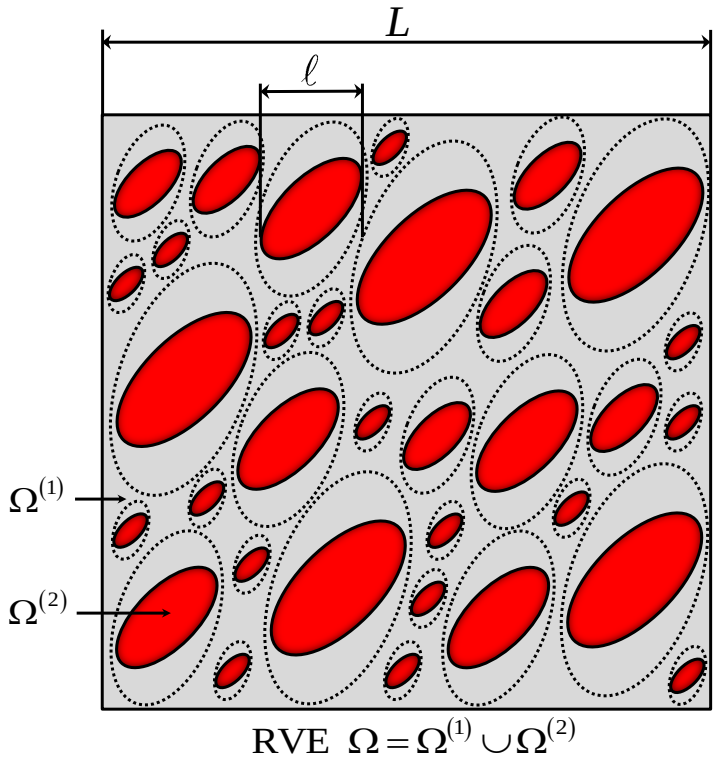

Figure 2.1: Representative volume element of a two-phase particulate composite consisting of aligned, ellipsoidal inclusions (solid lines) that are distributed with a different ellipsoidal symmetry (dotted lines) in a matrix material.

Under the above mentioned hypotheses of statistical uniformity and separation of length-scales, it is expected that the RVE will behave macroscopically as homogeneous. This in turn implies that macroscopically uniform fields will occur when an affine boundary condition is applied at the boundary $\partial\Omega$ of the RVE. Therefore, in order to determine the effective behavior of the composite we consider the boundary condition of uniform traction

$$\boldsymbol{\sigma}(\mathbf{x}) \cdot \mathbf{n}(\mathbf{x}) = \overline{\boldsymbol{\sigma}} \cdot \mathbf{n}(\mathbf{x}), \tag{2.5}$$

where $\overline{\boldsymbol{\sigma}}$ is a constant, symmetric, second-order tensor and $\mathbf{n}(\mathbf{x})$ is the outward unit vector normal to $\partial\Omega$. It follows from the divergence theorem that under this boundary condition the resulting macroscopic, or average stress field over the RVE is

$$\langle \boldsymbol{\sigma} \rangle = \overline{\boldsymbol{\sigma}}. \tag{2.6}$$

Thus, the effective behavior of the composite may be determined from the relation between the imposed uniform stress and the produced macroscopic strain.

Given the boundary condition (2.5) and assuming no body forces, the effective stress potential of the two-phase medium is defined directly from the principle of minimum potential energy as (Hill, 1963 [12]; Suguet, 1987 [25]; Ponte Castañeda and Suquet, 1998 [22]):

$$\widetilde{u}(\overline{\boldsymbol{\sigma}}) \equiv \min_{\boldsymbol{\tau} \in \mathcal{S}(\overline{\boldsymbol{\sigma}})} \langle u(\mathbf{x}, \boldsymbol{\tau}) \rangle = \min_{\boldsymbol{\tau} \in \mathcal{S}(\overline{\boldsymbol{\sigma}})} \sum_{r=1}^{2} c^{(r)} \, \langle u^{(r)}(\boldsymbol{\tau}) \rangle^{(r)}, \tag{2.7}$$

where

$$\mathcal{S}(\overline{\boldsymbol{\sigma}}) = \left\{ \boldsymbol{\tau}, \nabla \cdot \boldsymbol{\tau} = 0 \text{ in V and } \langle \boldsymbol{\tau} \rangle = \overline{\boldsymbol{\sigma}} \right\} \tag{2.8}$$

is the associated statically admissible set of stress fields $\boldsymbol{\tau}$ over Ω, that are divergence free and satisfy the boundary condition (2.5), while $\boldsymbol{\sigma}$ is the actual stress field over the RVE that minimizes the stress functional. It follows then, that the effective constitutive relation is given by

$$\overline{\boldsymbol{\epsilon}} = \frac{\partial \widetilde{u}}{\partial \overline{\boldsymbol{\sigma}}}(\overline{\boldsymbol{\sigma}}), \tag{2.9}$$

where $\overline{\boldsymbol{\epsilon}} \equiv \langle \boldsymbol{\epsilon} \rangle$ is the corresponding average strain over Ω.

Alternatively, the homogenization problem can be formulated by using the strain potentials $w^{(r)}(\boldsymbol{\epsilon})$ of the phases, that are related to the stress potentials $u^{(r)}(\boldsymbol{\sigma})$ by means of the the Legendre-Fenchel transformation

$$w^{(r)}(\boldsymbol{\epsilon}) = (u^{(r)})^*(\boldsymbol{\epsilon}) = \max_{\boldsymbol{\sigma}} \left[\boldsymbol{\sigma} : \boldsymbol{\epsilon} - u^{(r)}(\boldsymbol{\sigma}) \right]. \tag{2.10}$$

The local constitutive relation is now given by the relation

$$\boldsymbol{\sigma} = \frac{\partial w}{\partial \boldsymbol{\epsilon}}(\mathbf{x}, \boldsymbol{\epsilon}), \quad w(\mathbf{x}, \boldsymbol{\epsilon}) = \sum_{r=1}^{N} \chi^{(r)}(\mathbf{x})\ w^{(r)}(\boldsymbol{\epsilon}) \tag{2.11}$$

and correspondingly, the effective response of the composite medium is given through the effective strain potential $\widetilde{w}(\overline{\boldsymbol{\epsilon}})$, defined as

$$\overline{\boldsymbol{\sigma}} = \frac{\partial \widetilde{w}}{\partial \overline{\boldsymbol{\epsilon}}}(\overline{\boldsymbol{\epsilon}}), \quad \widetilde{w}(\overline{\boldsymbol{\epsilon}}) \equiv \min_{\boldsymbol{\epsilon} \in \mathcal{K}(\overline{\boldsymbol{\epsilon}})} \langle w(\mathbf{x}, \boldsymbol{\epsilon}) \rangle = \min_{\boldsymbol{\epsilon} \in \mathcal{K}(\overline{\boldsymbol{\epsilon}})} \sum_{r=1}^{2} c^{(r)}\ \langle w^{(r)}(\boldsymbol{\epsilon}) \rangle^{(r)}, \tag{2.12}$$

where $\mathcal{K}(\overline{\boldsymbol{\epsilon}})$ is the kinematically admissible set of strain fields, such that there is a continuous displacement field $\mathbf{u}$ satisfying $\boldsymbol{\epsilon} = (\nabla \mathbf{u} + (\nabla \mathbf{u})^T)/2$ in Ω and the condition $\mathbf{u} = \overline{\boldsymbol{\epsilon}} \cdot \mathbf{x}$ on $\partial\Omega$. Finally, it should be remarked that under the convexity assumption the effective potentials $\widetilde{u}(\overline{\boldsymbol{\sigma}})$ and $\widetilde{w}(\overline{\boldsymbol{\epsilon}})$ are also convex functions and that the formulations (2.7) and (2.12) are equivalent in the sense that the effective potentials are Legendre duals of each other (Ponte Castañeda and Willis, 1988[17]).

2.2 Linear-elastic composites

For the special case of materials with linear elastic behavior, the stress is related with the strain linearly via the constitutive relation

$$\boldsymbol{\sigma} = \frac{\partial w^{(r)}(\boldsymbol{\epsilon})}{\partial \boldsymbol{\epsilon}} = \mathbb{C}^{(r)} : \boldsymbol{\epsilon} \qquad \text{or} \qquad \boldsymbol{\epsilon} = \frac{\partial u^{(r)}(\boldsymbol{\sigma})}{\partial \boldsymbol{\sigma}} = \mathbb{S}^{(r)} : \boldsymbol{\sigma}, \tag{2.13}$$

where $\mathbb{C}^{(r)}$ and $\mathbb{S}^{(r)} = (\mathbb{C}^{(r)})^{-1}$ stand respectively for the elasticity (or stiffness) tensor and the compliance tensor of phase r, both being positive definite, fourth order tensors that

possess major and minor symmetries. It then follows, that the corresponding strain and stress potentials of the phases specialize to the following quadratic form

$$w^{(r)}(\boldsymbol{\epsilon}) = \frac{1}{2}\boldsymbol{\epsilon} : \mathbb{C}^{(r)} : \boldsymbol{\epsilon} \quad \text{and} \quad u^{(r)}(\boldsymbol{\sigma}) = \frac{1}{2}\boldsymbol{\sigma} : \mathbb{S}^{(r)} : \boldsymbol{\sigma}. \tag{2.14}$$

Furthermore, from the linearity of problem follows that the stress and strain fields must be linear to the applied boundary condition. This implies that the overall mean stress $\overline{\boldsymbol{\sigma}}$ is also related linearly to the overall mean strain $\overline{\boldsymbol{\epsilon}}$

$$\overline{\boldsymbol{\sigma}} = \widetilde{\mathbb{C}} : \overline{\boldsymbol{\epsilon}} \quad \text{and} \quad \overline{\boldsymbol{\epsilon}} = \widetilde{\mathbb{S}} : \overline{\boldsymbol{\sigma}}, \tag{2.15}$$

and, therefore, the relevant effective-strain and effective-stress potentials are of the form

$$\widetilde{w}(\overline{\boldsymbol{\epsilon}}) = \frac{1}{2}\overline{\boldsymbol{\epsilon}} : \widetilde{\mathbb{C}} : \overline{\boldsymbol{\epsilon}} \quad \text{and} \quad \widetilde{u}(\overline{\boldsymbol{\sigma}}) = \frac{1}{2}\overline{\boldsymbol{\sigma}} : \widetilde{\mathbb{S}} : \overline{\boldsymbol{\sigma}}, \tag{2.16}$$

where $\widetilde{\mathbb{C}}$ and $\widetilde{\mathbb{S}}$ are the associated effective elasticity and compliance tensor, such that $\widetilde{\mathbb{C}} = \widetilde{\mathbb{S}}^{-1}$. Similarly, the first moments, or averages of the stress and strain fields over each phase r, are linked to the macroscopic stress and strain respectively, through the linear equations

$$\overline{\boldsymbol{\sigma}}^{(r)} \equiv \langle \boldsymbol{\sigma} \rangle^{(r)} = \mathbb{B}^{(r)} : \overline{\boldsymbol{\sigma}} \quad \text{and} \quad \overline{\boldsymbol{\epsilon}}^{(r)} \equiv \langle \boldsymbol{\epsilon} \rangle^{(r)} = \mathbb{A}^{(r)} : \overline{\boldsymbol{\epsilon}}. \tag{2.17}$$

In the above expressions the quantities $\mathbb{B}^{(r)}$ and $\mathbb{A}^{(r)}$ denote the stress- and strain- concentration tensors that exhibit minor symmetry, but not necessarily major symmetry. Next, by making use of the fact that

$$\overline{\boldsymbol{\sigma}} = \sum_{r=1}^{2} c^{(r)} \overline{\boldsymbol{\sigma}}^{(r)} \quad \text{and} \quad \overline{\boldsymbol{\epsilon}} = \sum_{r=1}^{2} c^{(r)} \overline{\boldsymbol{\epsilon}}^{(r)} \tag{2.18}$$

it follows that the concentration tensors should satisfy the identities

$$\sum_{r=1}^{2} c^{(r)} \mathbb{B}^{(r)} = \mathbb{I} \quad \text{and} \quad \sum_{r=1}^{2} c^{(r)} \mathbb{A}^{(r)} = \mathbb{I}. \tag{2.19}$$

Also, from the constitutive relations for the phases follows that

$$\overline{\boldsymbol{\sigma}}^{(r)} = \mathbb{C}^{(r)} : \overline{\boldsymbol{\epsilon}}^{(r)} \quad \text{and} \quad \overline{\boldsymbol{\epsilon}}^{(r)} = \mathbb{S}^{(r)} : \overline{\boldsymbol{\sigma}}^{(r)}. \tag{2.20}$$

Then, by combining this last relations with (2.17) and (2.15) we obtain the following expressions for the effective elasticity and compliance tensors in terms of the associated stress- and strain-concentration tensors

$$\widetilde{\mathbb{S}} = \sum_{r=1}^{2} c^{(r)} \mathbb{S}^{(r)} : \mathbb{B}^{(r)} \quad \text{and} \quad \widetilde{\mathbb{C}} = \sum_{r=1}^{2} c^{(r)} \mathbb{C}^{(r)} : \mathbb{A}^{(r)}. \tag{2.21}$$

In addition, expressions for the second moments of the stress and strain in phase r can be obtained by differentiating the effective-stress and -strain potentials with respect to the elasticity and compliance tensor of the relevant phase

$$\langle \boldsymbol{\sigma} \otimes \boldsymbol{\sigma} \rangle^{(r)} = \frac{1}{c^{(r)}} \frac{\partial (\overline{\boldsymbol{\sigma}} : \widetilde{\mathbb{S}} : \overline{\boldsymbol{\sigma}})}{\partial \mathbb{S}^{(r)}} \quad \text{and} \quad \langle \boldsymbol{\epsilon} \otimes \boldsymbol{\epsilon} \rangle^{(r)} = \frac{1}{c^{(r)}} \frac{\partial (\overline{\boldsymbol{\epsilon}} : \widetilde{\mathbb{C}} : \overline{\boldsymbol{\epsilon}})}{\partial \mathbb{C}^{(r)}}. \tag{2.22}$$

Note, however, that if the stress and and strain fields are uniform over the phase r, the expressions $(2.22)_1$ and $(2.22)_2$ reduce respectively to

$$\langle \boldsymbol{\sigma} \otimes \boldsymbol{\sigma} \rangle^{(r)} = \overline{\boldsymbol{\sigma}}^{(r)} \otimes \overline{\boldsymbol{\sigma}}^{(r)} \quad \text{and} \quad \langle \boldsymbol{\epsilon} \otimes \boldsymbol{\epsilon} \rangle^{(r)} = \overline{\boldsymbol{\epsilon}}^{(r)} \otimes \overline{\boldsymbol{\epsilon}}^{(r)}. \tag{2.23}$$

Chapter 3

Estimates for the effective behavior of particulate composites

3.1 Linear-elastic composite

3.1.1 Dilute suspensions of particles

A major contribution to the theory of heterogeneous media has been made by Eshelby(1957 [6]), who solved the problem of a linear elastic, ellipsoidal inclusion embedded in a different linear elastic, infinite matrix material when the matrix is subject to a generic uniform strain (or stress) at infinity.

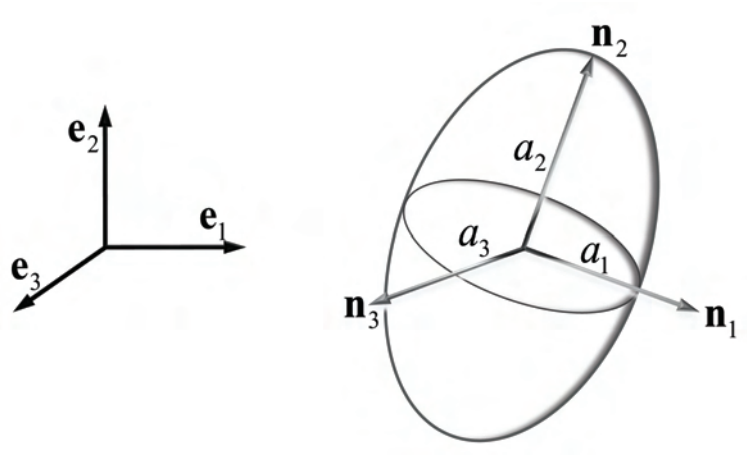

Figure 3.1: Geometrical Features of an Ellipsoid.

In this connection, we recall that the geometrical features of an ellipsoidal (see Fig. 3.1) may be defined as follows

$$\Omega_Z = \left\{ \mathbf{x}, |\boldsymbol{Z}^{-T} \cdot \mathbf{x}| \leq 1 \right\} \tag{3.1}$$

where $\boldsymbol{Z}$ is a symmetric, positive definite, second order tensor, which defines the shape and orientation of the ellipsoid and it is given by

$$\boldsymbol{Z} = \alpha_1 \mathbf{n}_1 \otimes \mathbf{n}_1 + \alpha_2 \mathbf{n}_2 \otimes \mathbf{n}_2 + \alpha_3 \mathbf{n}_3 \otimes \mathbf{n}_3 \tag{3.2}$$

with α_i and $\mathbf{n}_i$ denoting the principal values and the principal axes of the ellipsoid. For future reference, it is useful to introduce the aspect ratios

$$w_1 = \frac{\alpha_3}{\alpha_1} \quad \text{and} \quad w_2 = \frac{\alpha_3}{\alpha_2} \tag{3.3}$$

that completely describe the shape of the inclusion.

Eshelby's solution is based on the fact that the stress and strain fields in the inclusion are uniform when the applied field at infinity is uniform. Consider an ellipsoidal particle with elasticity tensor $\mathbb{C}^{(1)}$ embedded in an infinite matrix with elasticity tensor $\mathbb{C}^{(0)}$, subject to a uniform strain $\overline{\boldsymbol{\epsilon}}$ at infinity. Eshelby has shown that the strain field inside the inclusion is given by

$$\overline{\boldsymbol{\epsilon}}^{(1)} = \left[\mathbb{I} + \mathbb{P}^{(0)} : \left(\mathbb{C}^{(1)} - \mathbb{C}^{(0)}\right)\right]^{-1} : \overline{\boldsymbol{\epsilon}} \tag{3.4}$$

where the $\mathbb{P}^{(0)}$ is a constant fourth-order tensor that has major and minor symmetries, and is given by the expression

$$\mathbb{P}^{(0)} = \frac{\det \boldsymbol{Z}}{4\pi} \int_{|\boldsymbol{\xi}|=1} \mathbb{H}^{(0)}(\boldsymbol{\xi}) \, |\boldsymbol{Z} \cdot \boldsymbol{\xi}|^{-3} dS, \tag{3.5}$$

where

$$H^{(0)}_{ijpq} = \left[\boldsymbol{K}^{(0)}(\boldsymbol{\xi})\right]^{-1}_{ip} \xi_j \xi_q|_{(ij)(pq)} \quad \text{and} \quad K^{(0)}_{ip} = C^{(0)}_{ijpq} \xi_j \xi_q, \tag{3.6}$$

with the brackets in $(3.6)_1$ denoting symmetrization with respect to the corresponding indices. It should also be emphasized that the micro-structural tensor $\mathbb{P}^{(0)}$, and therefore the strain field $\overline{\boldsymbol{\epsilon}}^{(1)}$, depends on the shape and orientation of the inclusion but not on its size.

This solution generalizes to the case of a dilute composite, where the state of the strain in any one particle in the composite medium under homogeneous boundary conditions is not affected by all the other particles. In particular, we consider a composite made up of a dilute suspension of ellipsoidal particles, with elasticity tensor $\mathbb{C}^{(1)}$, distributed in a homogeneous matrix, with elasticity tensor $\mathbb{C}^{(0)}$, as shown in Fig.3.2. The inclusions are randomly distributed in the matrix in a way that the resulting composite is macroscopically uniform, and their shape and orientation is assumed to be characterized by identical shape tensors $\boldsymbol{Z}^{(1)}_i$. Then, it follows from Eshelby's solution that the strain-concentration tensor for the inclusion phase is given by

$$\mathbb{A}^{(1)} = \left[\mathbb{I} + \mathbb{P}^{(0)} : \left(\mathbb{C}^{(1)} - \mathbb{C}^{(0)}\right)\right]^{-1} \quad , \tag{3.7}$$

where $\mathbb{P}^{(0)}$ is the associated micro-structure tensor. Next, taking into account the identity (2.19) and the relation (2.21), we obtain the following expression for the effective elasticity tensor of the above described dilute composite

$$\widetilde{\mathbb{C}} = \mathbb{C}^{(0)} + c^{(1)} \left[\left(\mathbb{C}^{(1)} - \mathbb{C}^{(0)}\right) + \mathbb{P}^{(0)}_i\right]^{-1} \tag{3.8}$$

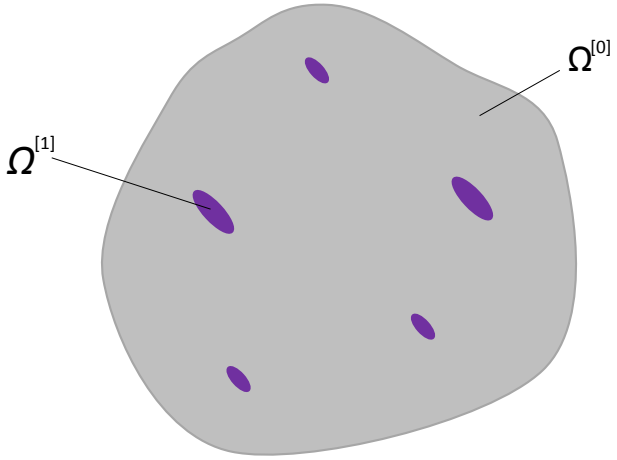

Figure 3.2: Schematic representation of a dilute composite (N=2).

3.1.2 Hashin-Shtrikman type of estimates

For a composite that it is not dilute, interactions between particles must be accounted for. Thus the homogenization problem of estimating the effective behavior becomes extremely difficult to solve. In order to deal with this problem, Hashin and Strickman [9] introduced a variational princibles which can be used to obtain bounds and estimates for composite materials with linear constituents. These principles were first used by HS to generate bounds for random composites with statistically isotropic microstructures. These bounds were generalized to random composite materials with more general ellipsoidal (anisotropic) microstructures by Willis [27]. Building on the work of Willis [27] Ponte Castañenda and Willis [18] developed more specific bounds and estimates for the class of particulate microstructures consisting of ellipsoidal particles that are distributed with ellipsoidal symmetry in the matrix. The latter results will be referred in this work as PCW estimates and are discussed in more detail in the sequel.

Fig. 2.1 depicts a specimen of the materials of interest consisting of aligned ellipsoidal inclusions (phase 2) that are distributed randomly with ellipsoidal symmetry in a homogeneous matrix (phase 1). The shape and orientation of the inclusions are described in terms of the shape tensor $\boldsymbol{Z}^{(p)}$ by means of the relation (3.1), and the two-point probability of finding a pair of inclusions located at $\mathbf{x}$ and $\mathbf{x}'$ depends on $\mathbf{x}-\mathbf{x}'$ through the combination

$$p^{(d)}(\mathbf{x}-\mathbf{x}') = p^{(d)}(|(\boldsymbol{Z}^{(d)})^{-T}\cdot(\mathbf{x}-\mathbf{x}')|) \tag{3.9}$$

where $\boldsymbol{Z}^{(d)}$ is the corresponding shape tensor that characterizes the shape and orientation of the ellipsoidal distribution. For this class of materials, variational estimates for the effective elasticity and compliance tensor $\widetilde{\mathbb{C}}$ and $\widetilde{\mathbb{C}} = (\widetilde{\mathbb{S}})^{-1}$ are given by (Ponte Castañeda and Willis, 1995 [18]):

$$\widetilde{\mathbb{C}}^{PCW} = \mathbb{C}^{(1)} + c^{(2)}\left[\left(\mathbb{C}^{(2)}-\mathbb{C}^{(1)}\right)^{-1} + c^{(1)}\mathbb{P}\right]^{-1} \tag{3.10}$$

and

$$\widetilde{\mathbb{S}}^{PCW} = \mathbb{S}^{(1)} + c^{(2)} \left[\left(\mathbb{S}^{(2)} - \mathbb{S}^{(1)} \right)^{-1} + c^{(1)} \mathbb{Q} \right]^{-1}. \tag{3.11}$$

Here $\mathbb{P}$ and $\mathbb{Q}$ are fourth-order tensors, containing information about the shape and distribution of the particles, defined as:

$$\mathbb{P} = \frac{1}{c^{(1)}} \left[\mathbb{P}^{(p)} - c^{(2)} \mathbb{P}^{(d)} \right] \quad \text{and} \quad \mathbb{Q} = \frac{1}{c^{(1)}} \left[\mathbb{Q}^{(p)} - c^{(2)} \mathbb{Q}^{(d)} \right] \tag{3.12}$$

with

$$\mathbb{Q}^{(s)} = \mathbb{C}^{(1)} - \mathbb{C}^{(1)} : \mathbb{P}^{(s)} : \mathbb{C}^{(1)}, \tag{3.13}$$

while the superscript s refers to either $s = p$ or $s = d$ and the associated tensor $\mathbb{P}^{(s)}$ was defined by relation (3.5). Note that the estimates (3.10) and (3.11) are equivalent in the sense that $\widetilde{\mathbb{C}}^{PCW} = (\widetilde{\mathbb{S}}^{PCW})^{-1}$. It should also be noted that if $\mathbb{C}^{(1)} \leq \mathbb{C}^{(2)}$ (in the sense of quadratic forms) then expression (3.10) provides a lower bound for $\widetilde{\mathbb{C}}$ and (3.11) provides an upper bound for $\widetilde{\mathbb{S}}$. On the other hand, if $\mathbb{C}^{(1)} \geq \mathbb{C}^{(2)}$ then expression (3.10) provides an upper bound for $\widetilde{\mathbb{C}}$ and (3.11) provides a lower bound for $\widetilde{\mathbb{S}}$

In the context of the estimates (3.10) and (3.11), the first moments of the stress $\boldsymbol{\sigma}$ and strain $\boldsymbol{\epsilon}$ over the inclusions of the composite are given by

$$\overline{\boldsymbol{\sigma}}^{(2)} = \mathbb{B}^{(2)} : \overline{\boldsymbol{\sigma}}, \quad \mathbb{B}^{(2)} = [\mathbb{I} + c^{(1)} \mathbb{Q} : (\mathbb{S}^{(2)} - \mathbb{S}^{(1)})]^{-1} \tag{3.14}$$

and

$$\overline{\boldsymbol{\epsilon}}^{(2)} = \mathbb{A}^{(2)} : \overline{\boldsymbol{\epsilon}}, \quad \mathbb{A}^{(2)} = [\mathbb{I} + c^{(1)} \mathbb{P} : (\mathbb{C}^{(2)} - \mathbb{C}^{(1)})]^{-1}. \tag{3.15}$$

In addition, making use of fact that the calculation of the above bounds was carried out by assuming that the fields in the inclusions are uniform, the expressions for the corresponding second moments reduces to

$$\langle \boldsymbol{\sigma} \otimes \boldsymbol{\sigma} \rangle^{(2)} = \overline{\boldsymbol{\sigma}}^{(2)} \otimes \overline{\boldsymbol{\sigma}}^{(2)} \quad \text{and} \quad \langle \boldsymbol{\epsilon} \otimes \boldsymbol{\epsilon} \rangle^{(2)} = \overline{\boldsymbol{\epsilon}}^{(2)} \otimes \overline{\boldsymbol{\epsilon}}^{(2)}. \tag{3.16}$$

In this work, we will use the PCW estimates to describe the effective behavior of linear-elastic particulate composites with isotropic phases. In this context, it should be noted that for composites with isotropic distribution of spherical particles, as well as for the case of isotropic distribution of aligned fibers with circular cross-sections the PCW estimates will take precisely the same form as the Hashin–Shtrikman [9] bounds. In particular, for a composite consisting of spherical particles ($w_1 = w_2 = 1$) that are distributed isotropically in a matrix material the Hashin and Shtrikman estimates for the effective shear and bulk modulus are respectively given by

$$\tilde{\mu}^{HS} = c^{(1)}\mu^{(1)} + c^{(2)}\mu^{(2)} - \frac{c^{(1)}c^{(2)}(\mu^{(1)} - \mu^{(2)})^2}{c^{(2)}\mu^{(1)} + c^{(1)}\mu^{(2)} + \mu^{(1)}\frac{8\mu^{(1)}+9\kappa^{(1)}}{6(2\mu^{(1)}+\kappa^{(1)})}} \tag{3.17}$$

and

$$\tilde{\kappa}^{HS} = c^{(1)}\kappa^{(1)} + c^{(2)}\kappa^{(2)} - \frac{c^{(1)}c^{(2)}(\kappa^{(1)} - \kappa^{(2)})^2}{c^{(2)}\kappa^{(1)} + c^{(1)}\kappa^{(2)} + 4\mu^{(1)}/3} \tag{3.18}$$

In addition, for an incompressible transversely isotropic composite consisting of aligned fibers of circular cross-section ($w_1 = w_2 = w, w \to \infty$) that are distributed isotropically

(isotropic symmetry in the transverse plane) in a matrix material the HS estimate for the associated in-plane (and anti-plane) effective shear modulus is given by

$$\tilde{\mu}_p^{HS} = \mu^{(1)} \frac{(1-c^{(2)})\mu^{(1)} + (1+c^{(2)})\mu^{(2)}}{(1+c^{(2)})\mu^{(1)} + (1-c^{(2)})\mu^{(2)}}. \tag{3.19}$$

Finally, as already mentioned, the stress and strain fields associated with the PCW estimate are uniform (by assumption) in phase 2, which, in general, is not true for composites beyond the dilute regime. However, we recall that for a dilute linear elastic composite, the stress and strain fields within the ellipsoidal inclusions turn out to be constant. This observation implies that the estimates (3.10) and (3.11) are exact for dilute composites where the particles are well separated, but on the other hand, for non-dilute concentration of inclusions their accuracy will decrease as the concentration of particles becomes higher.

3.2 Nonlinear composites: The variational procedure of Ponte Castañeda

In this section we will present the variational method proposed by Ponte Castañeda [19, 20] which can be used to obtain bounds and estimates for the properties of nonlinear composites. Specifically, this method makes use of a suitable chosen linear comparison composite (LCC) to estimate the effective properties of a nonlinear composite in terms of already available estimates for the corresponding linear composite.

We consider a nonlinear two-phase composite material with random particulate microstructure consisting of aligned ellipsoidal inclusions that are distributed with ellipsoidal symmetry in a matrix material. The constitutive behavior of the nonlinear phases is characterized by convex stress potentials $u^{(r)}$, satisfying the conditions $u^{(r)}(\mathbf{0}) = 0$ and $u^{(r)}(\boldsymbol{\sigma}) \to \infty$ as $|\boldsymbol{\sigma}| \to \infty$

The estimate for the macroscopic stress potential of the above described composite has as follows

$$\widetilde{u}(\overline{\boldsymbol{\sigma}}) \approx \widetilde{u}^{VB}(\overline{\boldsymbol{\sigma}}) \tag{3.20}$$

with

$$\widetilde{u}^{VB}(\overline{\boldsymbol{\sigma}}) = \sup_{\mathbb{S}^{(1)},\, \mathbb{S}^{(2)}} \left[\frac{1}{2} \overline{\boldsymbol{\sigma}} : \widetilde{\mathbb{S}} : \overline{\boldsymbol{\sigma}} - \sum_{r=1}^{2} c^{(r)} v^{(r)} \left(\mathbb{S}^{(r)} \right) \right], \tag{3.21}$$

where the "error functions" $v^{(r)}$ are defined by

$$v^{(r)}(\mathbb{S}^{(r)}) = \sup_{\hat{\boldsymbol{\sigma}}^{(r)}} \left[\frac{1}{2} \hat{\boldsymbol{\sigma}}^{(r)} : \mathbb{S}^{(r)} : \hat{\boldsymbol{\sigma}}^{(r)} - u^{(r)}(\hat{\boldsymbol{\sigma}}^{(r)}) \right]. \tag{3.22}$$

In the above equations the tensor $\widetilde{\mathbb{S}}$ denotes the effective compliance tensor of a "linear comparison composite" LCC which has the same microstructure as the actual nonlinear material, while $\mathbb{S}^{(1)}$ and $\mathbb{S}^{(2)}$ are the compliance tensors that define the local constitutive relation of the phases of the LCC and $\hat{\boldsymbol{\sigma}}^{(r)}$ are second-order tensors, that maximize the corrector functions $v^{(r)}$. The discussion of the optimality conditions in (3.21) and (3.22),

will not be performed here in the general context, but instead we will assume that the potentials $u^{(r)}$ are incompressible and isotropic functions of the form

$$u^{(r)}(\boldsymbol{\sigma}) = \psi^{(r)}(\sigma_e) \equiv g^{(r)}(\sigma_e^2), \tag{3.23}$$

where $\sigma_e = \sqrt{3\boldsymbol{\sigma}_d : \boldsymbol{\sigma}_d/2}$ denotes the von Misses equivalent stress, and $g^{(r)}$ are non negative convex functions of σ_e^2 such that $g^{(r)} \to \infty$ as $\sigma_e^2 \to \infty$. Then, the corresponding properties of the matrix and the particle phase of the LCC are assumed to be of the form

$$\mathbb{S}^{(r)} = \frac{1}{2\mu^{(r)}}\mathbb{K}. \tag{3.24}$$

The optimality conditions in (3.21) and (3.22) generate now the following system of nonlinear equations

$$\hat{\sigma}^{(r)} = \sqrt{\langle \sigma_e^2 \rangle^{(r)}} = \sqrt{\frac{3}{2c^{(r)}}\overline{\boldsymbol{\sigma}} : \frac{\partial \widetilde{\mathbb{S}}}{\partial \left(2\mu^{(r)}\right)^{-1}} : \overline{\boldsymbol{\sigma}}} \tag{3.25}$$

and

$$\frac{1}{2\mu^{(r)}} = \frac{3\psi^{(r)'}(\hat{\sigma}^{(r)})}{2\hat{\sigma}^{(r)}}, \tag{3.26}$$

where $\hat{\sigma}^{(r)}$ corresponds to the second moment of the equivalent stress field in phase r of the LCC, and are determined along with the the scalar moduli $\mu^{(r)}$. Finally, using the result (3.25), the estimate (3.21) can be rewritten as

$$\widetilde{u}^{VB}(\overline{\boldsymbol{\sigma}}) = (1 - c^{(2)})\psi^{(1)}(\hat{\sigma}^{(1)}) + c^{(2)}\psi^{(2)}(\hat{\sigma}^{(2)}) \tag{3.27}$$

In addition, for the special case that the particles are distributed isotropically, it turns out that that the homogenized potential of the composite (3.27) is also of the form (3.23) [1], i.e.

$$\tilde{u}(\overline{\boldsymbol{\sigma}}) = \tilde{\psi}(\overline{\sigma}_e) \equiv \tilde{g}(\overline{\sigma}_e^2), \tag{3.28}$$

where the function $\tilde{g}$ posses the same properties as $g^{(r)}$. The optimality condition (3.25) may now be written as

$$\hat{\sigma}^{(r)} = \sqrt{\langle \sigma_e^2 \rangle^{(r)}} = \sqrt{\frac{1}{c^{(r)}}\frac{\partial(2\tilde{\mu})^{-1}}{\partial \left(2\mu^{(r)}\right)^{-1}}\overline{\sigma}_e^2}, \tag{3.29}$$

where we have made use of the fact that

$$\widetilde{\mathbb{S}} = \frac{1}{2\tilde{\mu}}\mathbb{K}. \tag{3.30}$$

However, as discussed earlier, estimating exactly the effective compliance tensor $\widetilde{\mathbb{S}}$ is not possible, in general. Therefore, in this work we will use the estimate (3.11) as an approximation for $\widetilde{\mathbb{S}}$. Next, assuming that the phases of the nonlinear composite are *well-ordered*, such that

$$u^{(1)}(\boldsymbol{\sigma}) \geq u^{(2)}(\boldsymbol{\sigma}), \tag{3.31}$$

it is expected that the phases of the LCC will also be well ordered $\mathbb{S}^{(1)} \geq \mathbb{S}^{(2)}$. In this case, the expression (3.11) will provide a lower bound for the effective compliance tensor $\widetilde{\mathbb{S}}$ of the LCC material, and in turn, the expression (3.21) will also provide a rigorous lower bound for the nonlinear medium. On the other hand, if an upper bound is used for $\widetilde{\mathbb{S}}$, the expression (3.21) provides only an estimate for $\tilde{u}(\overline{\boldsymbol{\sigma}})$.

Chapter 4

The incremental homogenization scheme

Another method for estimating the effective properties of linear composites with particulate microstructures, is the Differential Scheme (DS), introduced first by Bruggeman [3] in the context of conductivity, and generalized later by Norris [15] to materials with more than two phases. The DS is based on the idea of the incremental construction of the composite by adding sequentially an infinitesimal amount of inclusions to the matrix material. The basic assumption is that the added inclusions at each stage of the construction process are much larger than the previous ones, thus the medium surrounding them can be treated as homogeneous. Since every volume increment is infinitesimal small, the new inclusions will be in a dilute suspension with respect to the effective medium of the previous level, therefore the effective properties of the composite at each stage of this iterative procedure may be computed using a dilute concentration result, such as (3.8). The essential problem with this method is that the corresponding microstructure is not realistic, since a composite having an infinite numbers of length scales could never be built in practice. However, as shown by Zimmerman [33] it frequently happens the effective properties computed with the DS to agree quite well with experimental data, although the details of the microstructure of the model and the tested specimen are different.

As discussed in the last paragraph of the subsection 3.1.2, the PCW estimates are exact estimates for dilute composites, but their accuracy is expected to deteriorate for high particles concentrations. Given this observation, it is then appropriate to investigate the possibility of obtaining estimates different and hopefully more accurate from their standard counterparts, by using a discretized version of the DS, where the composite is constructed incrementally by the gradual addition of a small, but non infinitesimal, amount of inclusions. In the next two subsections, we will describe the incremental homogenization procedure that we will use in this work in the context of linear and nonlinear particulate composites.

4.1 Incremental homogenization for linear-elastic composites

In this section, we will use the discretized version of the DS to estimate the effective response of a two-phase, linear-elastic composite material, consisting of ellipsoidal inclusions with elasticity tensor $\mathbb{C}^{(2)}$ embedded in a homogeneous matrix with elasticity tensor $\mathbb{C}^{(1)}$. Following Agoras and Ponte Castañeda [1], we consider an N-scale particulate composite, as shown schematically in Fig. 4.1, which may be constructed by means of the following iterative procedure. At the first stage of the iterative procedure, we add a small volume fraction $c^{(2)}_{[1]}$ of ellipsoidal particles to the homogeneous matrix, that are distributed randomly with ellipsoidal symmetry, where the two-point correlation function of the particle distribution has the same aspect ratio and orientation of those of the particles, such that $\boldsymbol{Z}^{(p)}_{[1]} = \boldsymbol{Z}^{(d)}_{[1]} = \boldsymbol{Z}$. Then, the PCW estimate (3.10) for the effective elasticity tensor of the resulting composite is given by

$$\widetilde{\mathbb{C}}^{IH}_{[1]} = \mathbb{C}^{(1)} + c^{(2)}_{[1]} \left[\left(\mathbb{C}^{(2)} - \mathbb{C}^{(1)} \right)^{-1} + (1 - c^{(2)}_{[1]}) \mathbb{P}_{[1]} \right]^{-1}, \tag{4.1}$$

where the label "IH" stands for Incremental Homogenization and with $\mathbb{P}_{[1]}$ given by (3.5) in terms of $\boldsymbol{Z}$ and $\mathbb{C}^{[1]}$. In the second iteration we add to the current composite medium a volume fraction $c^{(2)}_{[2]}$ of even larger ellipsoidal particles, with inclusion and distribution shapes that are identical to the particles at the first iteration ($\boldsymbol{Z}^{(p)}_{[2]} = \boldsymbol{Z}^{(d)}_{[2]} = \boldsymbol{Z}$). The resulting composite may now be treated as a two-phase, single-scale composite with one matrix phase with elasticity tensor $\widetilde{\mathbb{C}}^{IH}_{[1]}$ and one inclusion phase with elasticity tensor $\mathbb{C}^{(2)}$. Thus, the PCW estimate (3.10) for the effective elasticity tensor $\widetilde{\mathbb{C}}^{IH}_{[2]}$ is given by

$$\widetilde{\mathbb{C}}^{IH}_{[2]} = \widetilde{\mathbb{C}}_{[1]} + c^{(2)}_{[2]} \left[\left(\mathbb{C}^{(2)} - \widetilde{\mathbb{C}}_{[1]} \right)^{-1} + (1 - c^{(2)}_{[2]}) \mathbb{P}_{[2]} \right]^{-1}. \tag{4.2}$$

The final composite is constructed by repeating this process N times, until we reach the desired volume fraction of particles, denoted as $c^{(2)}$. Now, the corresponding expression for the effective stiffness tensor of the composite is

$$\widetilde{\mathbb{C}}^{IH}_{[N]} = \widetilde{\mathbb{C}}^{IH}_{[N-1]} + c^{(2)}_{[N]} \left[\left(\mathbb{C}^{(2)} - \widetilde{\mathbb{C}}^{IH}_{[N-1]} \right)^{-1} + (1 - c^{(2)}_{[N]}) \mathbb{P}_{[N]} \right]^{-1}, \tag{4.3}$$

and the total concentration of particles in the final material may be expressed as

$$c^{(2)} = 1 - \prod_{i=1}^{N} (1 - c^{(2)}_{[i]}) \tag{4.4}$$

where $c^{(2)}_{[i]}$ represents the volume fraction of the inclusions added at the i-th stage.

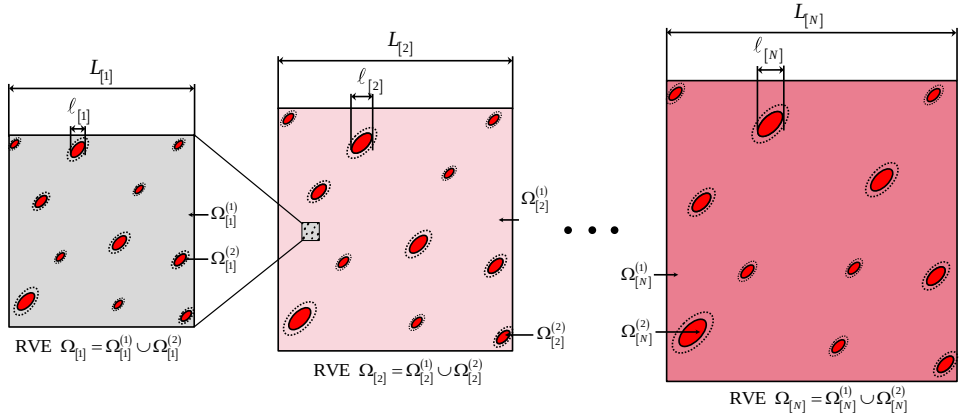

Figure 4.1: Schematic of a *self-similar* microstructure. RVE $\Omega_{[1]}$: ellipsoidal inclusions are distributed with ellipsoidal symmetry in a homogeneous matrix material. RVE $\Omega_{[i]}$ with $i = 2, ..., N$: ellipsoidal inclusions are distributed with ellipsoidal symmetry in a heterogeneous matrix composed of the material in RVE $\Omega_{[i-1]}$.

4.2 Incremental homogenization for nonlinear composites

In this section we use the IH scheme to estimate the effective behavior of a nonlinear composite, consisting of two isotropic phases. The construction process is the same as described in the previous section, starting with the smallest inclusions and proceeds with increasing orders of magnitude. Again, we will assume that at each stage of the construction process both the inclusions and their distribution function have the same ellipsoidal shape and orientation. However, for simplicity, we will present the incremental procedure for statistically isotropic microstructures, i.e $\boldsymbol{Z} = \mathbf{I}$, so that the material of the matrix phase will remain isotropic in every level of the composite. The corresponding microstructure is now depicted in Fig. 5.1.

Although more general constitutive models for the phases may be used, in this work for simplicity the constitutive behavior of the matrix and the inclusion phase is taken to be isotropic and incompressible, characterized by the stress potentials of the form (3.23), i.e.,

$$u^{(r)}(\boldsymbol{\sigma}) = \psi^{(r)}(\sigma_e) \equiv g^{(r)}(\sigma_e^2) \tag{4.5}$$

where we recall that $\sigma_e = \sqrt{3\boldsymbol{\sigma}_d : \boldsymbol{\sigma}_d/2}$ and that $\boldsymbol{\sigma}_d$ denotes the deviatoric part of the stress tensor. The $g^{(r)}$ are assumed to be non-negative, convex functions of σ_e^2 , such that $g^{(r)} \to \infty$ as $\sigma_e^2 \to \infty$. In addition, the fact that the microstructures under consideration are statistically isotropic implies that the homogenized potential of each level of the composite will also be of the form (4.5) [1]

We begin by making use of the expression (3.21) to obtain the following estimate for the effective stress potential of the level-1 material

$$\widetilde{u}_{[1]}^{IH}(\overline{\boldsymbol{\sigma}}_{[1]}) = \tilde{\psi}_{[1]}(\overline{\sigma}_{e[1]}) = c_{[1]}^{(1)}\psi^{(1)}(\hat{\sigma}_{[1]}^{(1)}) + c_{[1]}^{(2)}\psi^{(2)}(\hat{\sigma}_{[1]}^{(2)}) \tag{4.6}$$

while from the optimality conditions (3.26) and (3.29) we have the following system of

nonlinear equations

$$\frac{1}{2\mu_{[1]}^{(r)}} = \frac{3\psi_{[1]}^{(r)'}(\hat{\sigma}_{[1]}^{(r)})}{2\hat{\sigma}_{[1]}^{(r)}}, \tag{4.7}$$

and

$$\hat{\sigma}_{[1]}^{(r)} = \sqrt{\langle \sigma_{e[1]}^2 \rangle^{(r)}} = \sqrt{\frac{1}{c_{[1]}^{(r)}} \frac{\partial(2\tilde{\mu}_{[1]})^{-1}}{\partial\big(2\mu_{[1]}^{(r)}\big)^{-1}} \overline{\sigma}_{e[1]}^2} \tag{4.8}$$

where we recall that $\hat{\sigma}_{[1]}^{(r)}$ is the second moment of the equivalent stress over the phase r of the LCC under an average applied stress $\overline{\boldsymbol{\sigma}}_{[1]}$ and $\overline{\sigma}_{e[1]}$ is the associated applied equivalent stress. Next, we use the same procedure to estimate the effective response of the material in $\Omega_{[2]}$

$$\widetilde{u}_{[2]}^{IH}(\overline{\boldsymbol{\sigma}}_{[2]}) = \tilde{\psi}_{[2]}(\overline{\sigma}_{e[2]}) = c_{[2]}^{(1)}\psi_{[2]}^{(1)}(\hat{\sigma}_{[2]}^{(1)}) + c_{[2]}^{(2)}\psi^{(2)}(\hat{\sigma}_{[2]}^{(2)}), \tag{4.9}$$

where $\psi_{[2]}^{(1)} = \tilde{\psi}_{[1]}$ and the associated optimality conditions are given by

$$\frac{1}{2\mu_{[2]}^{(r)}} = \frac{3\psi_{[2]}^{(r)'}(\hat{\sigma}_{[2]}^{(r)})}{2\hat{\sigma}_{[2]}^{(r)}}, \tag{4.10}$$

$$\hat{\sigma}_{[2]}^{(r)} = \sqrt{\langle \sigma_{e[2]}^2 \rangle^{(r)}} = \sqrt{\frac{1}{c_{[2]}^{(r)}} \frac{\partial(2\tilde{\mu}_{[2]})^{-1}}{\partial\big(2\mu_{[2]}^{(r)}\big)^{-1}} \overline{\sigma}_{e[2]}^2} \tag{4.11}$$

Note that the expression (4.9) implies that the second moments $\hat{\sigma}_{[1]}^{(r)}$ are evaluated at $\overline{\sigma}_{e[1]} = \hat{\sigma}_{[2]}^{(1)}$. Now, by substituting relation (4.6) in relation (4.9), we obtain

$$\begin{aligned}\widetilde{u}_{[2]}^{IH}(\overline{\boldsymbol{\sigma}}_{[2]}) &= c_{[2]}^{(1)}c_{[1]}^{(1)}\psi^{(1)}(\hat{\sigma}_{[1]}^{(1)}) + c_{[2]}^{(1)}c_{[1]}^{(2)}\psi^{(2)}(\hat{\sigma}_{[1]}^{(2)}) + c_{[2]}^{(2)}\psi^{(2)}(\hat{\sigma}_{[2]}^{(2)}) \\ &= \prod_{i=1}^{2}(1-c_{[i]}^{(2)})\psi^{(1)}(\hat{\sigma}_{[1]}^{(1)}) + \sum_{i=1}^{2} c_{[i]}^{(2)}\left(\prod_{j=i+1}^{2}(1-c_{[j]}^{(2)})\right)\psi^{(2)}(\hat{\sigma}_{[i]}^{(2)}),\end{aligned} \tag{4.12}$$

where we have used the fact that $c_{[i]}^{(1)} = 1 - c_{[i]}^{(2)}$. This procedure is repeated N times until we reach the final level-N composite, with the desired concentration of particles that is given by the relation (4.4). The corresponding IH estimate for the overall effective stress potential may be written in the form

$$\widetilde{u}_{[N]}^{IH}(\overline{\boldsymbol{\sigma}}) = \prod_{i=1}^{N}(1-c_{[i]}^{(2)})\psi^{(1)}(\hat{\sigma}_{[1]}^{(1)}) + \sum_{i=1}^{N} c_{[i]}^{(2)}\left(\prod_{j=i+1}^{N}(1-c_{[j]}^{(2)})\right)\psi^{(2)}(\hat{\sigma}_{[i]}^{(2)}), \tag{4.13}$$

and the associated optimality conditions at each stage of this iterative process are expressed as

$$\frac{1}{2\mu_{[i]}^{(r)}} = \frac{3\psi_{[i]}^{(r)'}(\hat{\sigma}_{[i]}^{(r)})}{2\hat{\sigma}_{[i]}^{(r)}} \tag{4.14}$$

and

$$\hat{\sigma}_{[i]}^{(r)} = \sqrt{\left\langle \sigma_{e[i]}^2 \right\rangle^{(r)}} = \sqrt{\frac{1}{c_{[i]}^{(r)}} \frac{\partial (2\tilde{\mu}_{[i]})^{-1}}{\partial \left(2\mu_{[i]}^{(r)}\right)^{-1}} \overline{\sigma}_{e[i]}^2}, \tag{4.15}$$

with $\psi_{[i]}^{(1)} = \widetilde{\psi}_{[i-1]}$, $\overline{\sigma}_{e[i]} = \hat{\sigma}_{[i+1]}^{(1)}$ and $\overline{\sigma}_{e[N]} = \overline{\sigma}_e$.

Chapter 5

Results and discussion

In this chapter, we will present some applications of the IH scheme for linear and nonlinear composites, within the context of 2-D and 3-D model problems, in order to explore the difference between one step and iterative homogenization. Specifically, in the 2-D examples we provide results for the effective in-plane response of composites consisting of aligned fibers of circular cross-section that are distributed isotropically in the transverse plane in a matrix material, and are subjected to plane-stress loading conditions. In the 3-D examples, we consider composites consisting of spherical particles that are distributed isotropically in a matrix material, and are subject to general loading conditions. These microstructures are shown schematically in Fig.5.1

Also, in this work we take the concentration of the inclusions to be the same for all length scales $c_{[i]}^{(2)} \equiv c$, thus the expression (4.4) may be rewritten in the form

$$c^{(2)} = 1 - (1 - c)^N \tag{5.1}$$

which implies that

$$c = 1 - (1 - c^{(2)})^{\frac{1}{N}}, \tag{5.2}$$

where we recall that $c^{(2)}$ is the total volume fraction og particles (or fibers) in the N-scale composite.

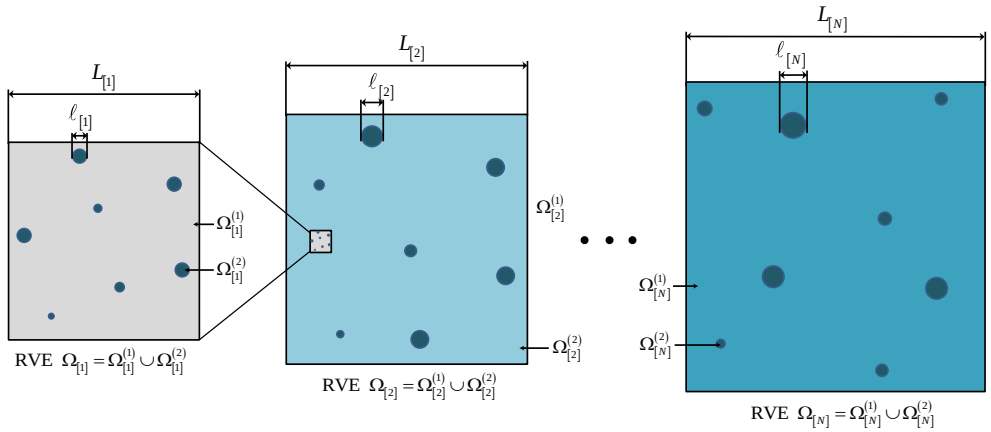

Figure 5.1: Schematic of a *self-similar* microstructure. RVE $\Omega_{[1]}$: spherical inclusions (or fibers of circular cross-section) are distributed in a homogeneous matrix material. RVE $\Omega_{[i]}$ with $i = 2, ..., N$: spherical inclusions (or fibers of circular cross-section) are distributed in a heterogeneous matrix composed of the material in RVE $\Omega_{[i-1]}$.

5.1 Linear elastic composites

5.1.1 Rigid particle composites

We will apply the iterative procedure of section 4.1 to a multi-scale linear elastic composite made up of spherical rigid inclusions embedded in an incompressible matrix material. We begin by using the expression (3.17) to estimate the effective shear modulus of the level-1 material

$$\tilde{\mu}^{IH}_{[1]} = \mu^{(1)} \frac{2+3c}{2(1-c)} \tag{5.3}$$

Next, we proceed to the second level of the composite. The separation of length scales hypothesis allows us to regard the material as a single scale composite but this time we take the matrix modulus to be the effective modulus of the previous level. The effective shear modulus in this step is

$$\tilde{\mu}^{IH}_{[2]} = \tilde{\mu}^{IH}_{[1]} \frac{2+3c}{2(1-c)} = \mu^{(1)} \left(\frac{2+3c}{2(1-c)} \right)^2 .$$

By iterating this procedure we get

$$\begin{aligned} \tilde{\mu}^{IH}_{[N]} &= \tilde{\mu}^{IH}_{[N-1]} \frac{2+3c}{2(1-c)} \\ &= \mu^{(1)} \left(\frac{2+3c}{2(1-c)} \right)^N \end{aligned}$$

and using (5.1), we get an expression for the effective shear modulus as a function of the overall particle concentration $c^{(2)}$

$$\tilde{\mu}^{IH}_{[N]} = \mu^{(1)} \left(\frac{5 - 3(1-c^{(2)})^{\frac{1}{N}})}{2(1-c^{(2)})^{\frac{1}{N}}} \right)^N . \tag{5.4}$$

For an infinite number of iterations $N \to \infty$, expression (5.4) reduces to

$$\tilde{\mu}^{IH}_{[\infty]} = \frac{1}{(1-c^{(2)})^{\frac{5}{2}}}. \tag{5.5}$$

It is noted that this IH estimate coincides with the corresponding estimate obtained by the differential scheme [33], as it should.

Fig. 5.2 presents results of the normalized effective shear modulus for increasing numbers of iterations. In particular, Fig. 5.2(a) shows plots for the normalized effective shear modulus for specific number of iterations $N = 1, 2, 10$ and $N \to \infty$, as a function of $c^{(2)}$. The deviation of these IH estimates from the corresponding HS estimate (which coincides with the IH for N=1) is shown in Fig.5.2(b), where the percent difference

$$d_{[N]} = 100\frac{\tilde{\mu}^{IH}_{[N]} - \tilde{\mu}^{HS}}{\tilde{\mu}^{HS}} \tag{5.6}$$

is plotted as a function of $c^{(2)}$. From Fig. 5.2(a) we observe that IH estimates for all values of N are greater that the HS estimate which is consistent with the bounding character of the latter. It is also observed that the estimates for $N = 100$ and $N \to \infty$ are indistinguishable, which suggests that practically the estimate converges for $N \simeq 100$

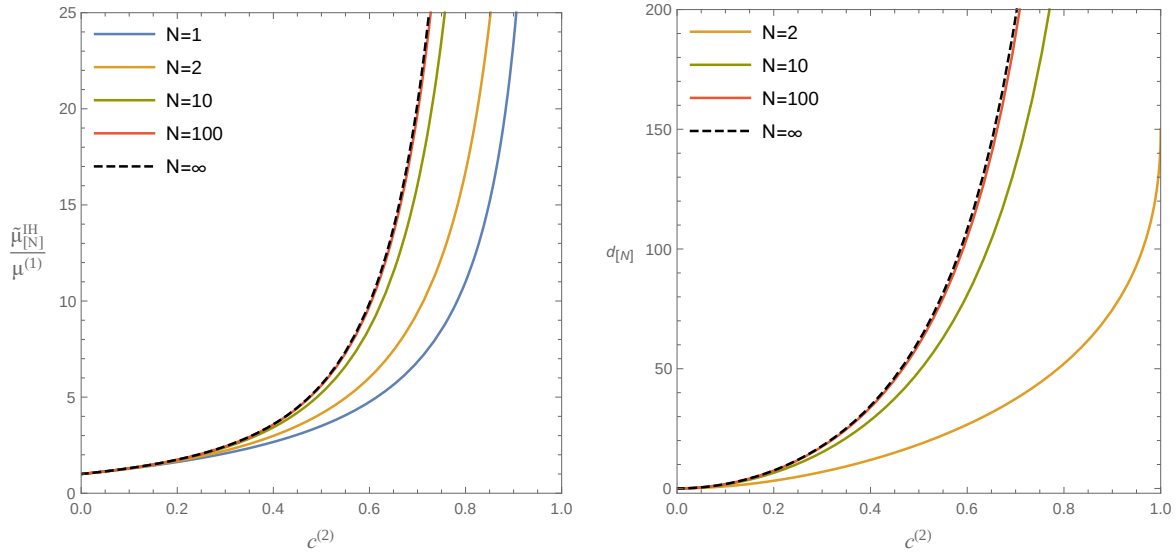

(a) (b)

Figure 5.2: IH estimates for the normalized effective shear modulus of a composite consisting of rigid spherical inclusions embedded in an isotropic, incompressible, linear elastic matrix are plotted as a function of the inclusion concentration.(a) The convergence of the IH estimate with increasing numbers (N) of increments, $N = 1, 2, 10, 100$ and $N \to \infty$ (b) The precentage difference $d_{[N]}$ between the IH estimate and the corresponding HS estimate for various values of N.

5.1.2 Porous composites

Consider a composite with the microstructure of Fig. 5.1, consisting of spherical voids (phase 2) embedded in an isotropic and incompressible matrix material (phase 1). The HS upper bound for the material described by the RVE $\Omega_{[1]}$ are

$$\tilde{\mu}^{IH}_{[1]} = \mu^{(1)}\frac{(1-c)}{1+\frac{2}{3}c} \qquad \text{and} \qquad \tilde{\kappa}^{IH}_{[1]} = \mu^{(1)}\frac{4}{3}\frac{(1-c)}{c} \tag{5.7}$$

Next, observing that the matrix material is compressible for $i = 2, ..., N$ we use expressions (3.17) and (3.18) to obtain the following results

$$\tilde{\mu}^{IH}_{[i]} = \tilde{\mu}^{IH}_{[i-1]}\left[(1-c) - \frac{(1-c)c}{c+\frac{8\tilde{\mu}^{IH}_{[i-1]}+9\tilde{\kappa}^{[IH]}_{[i-1]}}{6(2\tilde{\mu}^{IH}_{[i-1]}+\tilde{\kappa}^{IH}_{[i-1]})}}\right] \tag{5.8}$$

and

$$\tilde{\kappa}^{IH}_{[i]} = \tilde{\kappa}^{IH}_{[i-1]}\left[(1-c) - \frac{(1-c)c}{c+\frac{4\tilde{\mu}^{IH}_{[i-1]}}{3\tilde{\kappa}^{IH}_{[i-1]}}}\right] \tag{5.9}$$

Finally, using (5.2), the effective shear and bulk modulus of the composite in terms of the overall concentration of voids may be written as

$$\tilde{\mu}^{IH}_{[N]} = \mu^{(1)}\frac{3(1-c^{(2)})^{\frac{1}{N}}}{5-2(1-c^{(2)})^{\frac{1}{N}}}\prod_{j=2}^{N}\left[(1-c^{(2)})^{\frac{1}{N}} - \frac{\left[1-(1-c^{(2)})^{\frac{1}{N}}\right](1-c^{(2)})^{\frac{1}{N}}}{1-(1-c^{(2)})^{\frac{1}{N}}+\frac{8\tilde{\mu}^{IH}_{[j-1]}+9\tilde{\kappa}^{IH}_{[j-1]}}{6(2\tilde{\mu}^{IH}_{[j-1]}+\tilde{\kappa}^{IH}_{[j-1]})}}\right] \tag{5.10}$$

$$\tilde{\kappa}^{IH}_{[N]} = \mu^{(1)}\frac{4(1-c^{(2)})^{\frac{1}{N}}}{3\left[1-(1-c^{(2)})^{\frac{1}{N}}\right]}\prod_{j=2}^{N}\left[(1-c^{(2)})^{\frac{1}{N}} - \frac{\left[1-(1-c^{(2)})^{\frac{1}{N}}\right](1-c^{(2)})^{\frac{1}{N}}}{1-(1-c^{(2)})^{\frac{1}{N}}+\frac{4\tilde{\mu}^{IH}_{[j-1]}}{3\tilde{\kappa}^{IH}_{[j-1]})}}\right] \tag{5.11}$$

Figure 5.3 presents results for the normalized effective shear modulus as a function of $c^{(2)}$. For comparison, we also include the corresponding estimates obtained by the DS [15, 33]

$$\frac{\tilde{\mu}}{\mu^{(1)}} = (1-c^{(2)})^2\left[2-(\frac{\tilde{\mu}}{\mu^{(1)}})^{\frac{3}{5}}\right]^{\frac{1}{3}} \tag{5.12}$$

From Fig.5.3(a) we observe that IH predicts overall a more compliant behavior for the porous material than the HS estimate. It is also observed that the IH and the DS curves are almost identical. Fig5.3(b) shows plots of the difference (in percentage) between the HS (N=1) estimate and the corresponding estimates from the DS and the IH. It is clearly observed again that the differences are minor for small concentration of the voids (see $c^{(2)} = 0.1$) but become significant for higher values of $c^{(2)}$.

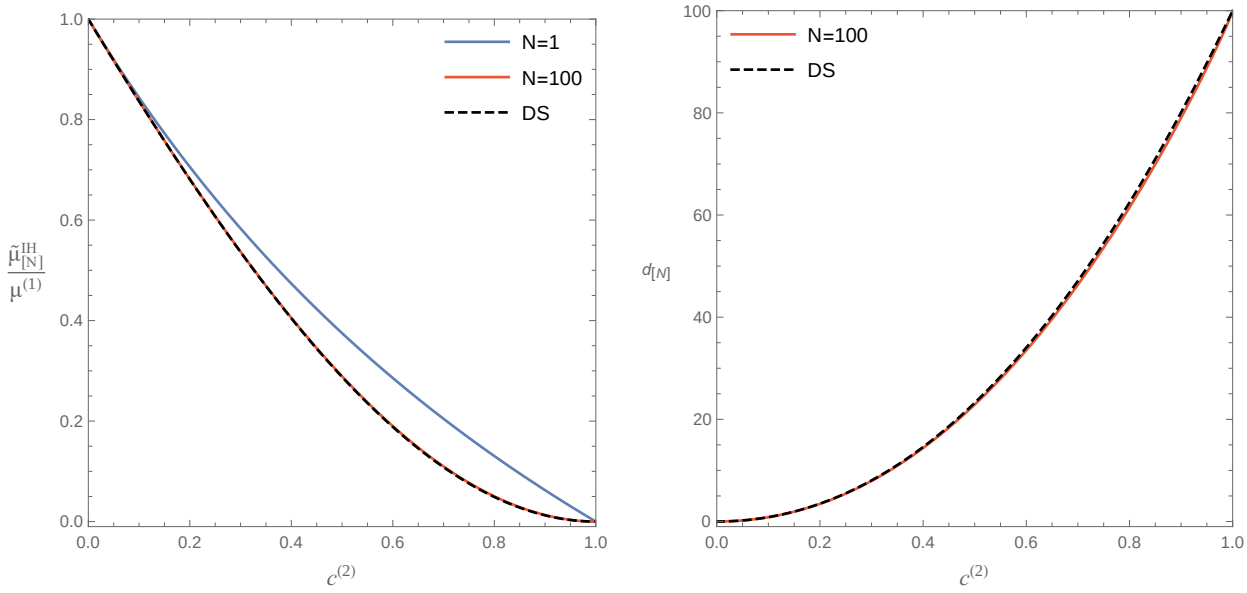

(a) (b)

Figure 5.3: Estimates for the normalized effective shear modulus of a composite consisting of spherical pores embedded in an isotropic, incompressible, linear elastic matrix are plotted as a function of the volume concentration of voids $c^{(2)}$. (a) The normalized effective shear modulus as predicted by the IH scheme compared with the homogenization estimates of the HS (N=1) bounds and the DS method. (b) The difference in percentage between the HS estimate and the corresponding estimates from the IH and the DS

5.1.3 Particle composites

In this subsection, we consider a composite consisting of incompressible and isotropic spherical particles, embedded in an incompressible and isotropic matrix phase. Taking the limit $\kappa^{(1)}_{[1]} \to \infty$ and $\kappa^{(2)}_{[1]} \to \infty$ in (3.17) it can be easily shown that the estimate for the effective shear modulus of the level-1 material is given by

$$\tilde{\mu}^{IH}_{[1]} = \mu^{(1)} \left[(1-c) + ct - \frac{(1-c)c(1-t)^2}{c + \frac{3}{2} + (1-c)t} \right], \tag{5.13}$$

where $t = \mu^{(2)}/\mu^{(1)}$ is the heterogeneity contrast. Then, the effective shear modulus in each stage of this iterative procedure is given by the following relation

$$\tilde{\mu}^{IH}_{[i]} = \tilde{\mu}_{[i-1]} \left[(1-c) + ct(\frac{\tilde{\mu}_{[i-1]}}{\mu^{(1)}})^{-1} - \frac{(1-c)c(1-t(\frac{\tilde{\mu}_{[i-1]}}{\mu^{(1)}})^{-1})^2}{c + \frac{3}{2} + (1-c)t(\frac{\tilde{\mu}_{[i-1]}}{\mu^{(1)}})^{-1}} \right], \tag{5.14}$$

Finally, using the expression (5.2) the overall effective shear modulus of the composite may be written as

$$\tilde{\mu}^{IH}_{[N]} = \mu^{(1)} \prod_{i=1}^{N} \left[\frac{3(1-c^{(2)})^{\frac{1}{N}} + \left[5 - 3(1-c^{(2)})^{\frac{1}{N}}\right] t(\frac{\tilde{\mu}_{[i-1]}}{\mu^{(1)}})^{-1}}{5 - 2(1-c^{(2)})^{\frac{1}{N}} + 2(1-c^{(2)})^{\frac{1}{N}} t(\frac{\tilde{\mu}_{[i-1]}}{\mu^{(1)}})^{-1}} \right] \tag{5.15}$$

Fig. 5.4 presents results for the effective shear modulus as a function of the particle concentration $c^{(2)}$. Specifically, Fig.5.4(a) provides plots for the effective shear modulus for a particle-weakened composite with a contrast $t = 0.2$, and Fig.5.4(c) for a particle reinforced composite with $t = 5$. We observe that in both cases the IH estimates are consistent with the HS (N=1) bounds. The deviation of these IH estimates from the corresponding HS estimates are shown in Fig.5.4(b) and Fig.5.4(d) where the percentage difference is plotted as a function of $c^{(2)}$. The main observation from these results is that the differences are much smaller than the differences observed in the previous cases. We also notice that the difference is slightly bigger when the inclusions are stiffer from the matrix. Finally, it is remarked that the the maximum difference in both cases occurs at about $c^{(2)} = 0.7$ while in the previous examples the maximum differences were observed at $c^{(2)} \to 1$.

5.1.4 Fiber composites

In this subsection we consider a fibrous, linear elastic, two-phase composite with the microstructure of Fig 5.1, subject to in-plane loadings. Both the matrix and fibers are assumed to be isotropic and incompressible. From the expression 3.19 we have that the estimate for the in-plane effective shear modulus of the level-1 material is given by

$$\tilde{\mu}^{IH}_{[1]} = \mu^{(1)} \frac{(1-c) + (1+c)t}{(1+c) + (1-c)t}, \tag{5.16}$$

where we recall that $t = \mu^{(2)}/\mu^{(1)}$ is the associated heterogeneity contrast. Then, following a similar procedure to the one described in the previous subsections, we arrive to the following result for the effective in-plane shear modulus of the composite

$$\tilde{\mu}^{IH}_{[N]} = \mu^{(1)} \prod_{i=1}^{N} \left[\frac{2\left[1 + t(\frac{\tilde{\mu}_{[i-1]}}{\mu^{(1)}})^{-1}\right]}{2 + (1-c^{(2)})^{\frac{1}{N}} \left[t(\frac{\tilde{\mu}_{[i-1]}}{\mu^{(1)}})^{-1} - 1\right]} - 1 \right].$$

For the extreme case of rigid fibers ($k \to \infty$) the above result reduces to

$$\tilde{\mu}^{IH}_{[N]} = \mu^{(1)} \left[2(1-c^{(2)})^{\frac{1}{N}}) - 1\right]^{N}, \tag{5.17}$$

which in the limit as $N \to \infty$ takes the form

$$\tilde{\mu}^{IH}_{[\infty]} = \mu^{(1)} \frac{1}{(1-c^{(2)})^2}. \tag{5.18}$$

Results for the normalized in-plane shear modulus are shown in Fig.5.5. Specifically, Fig.5.5(a) provides plots of the effective shear modulus for a fiber-weakened composite, $t = 0.2$, while Fig.5.5(c) for a fiber-reinforced composite with $t = 5$. The percentage difference of the IH estimates from the corresponding HS bounds (N=1) are plotted as a function of $c^{(2)}$ in Figs 5.5(b) and 5.5(d). As in the previous cases, the differences of the IH from the corresponding HS estimates are overall quite small, with a maximum close to $c^{(2)} = 0.7$. We also note that the IH results are consistent with the HS bounds.

Figoure 5.6 provides results for the IH estimates for the effective in-plane response of an incompressible composite reinforced with rigid fibers. From 5.6(a) we observe that in this case there are significant differences between the IH and HS estimates, albeit smaller than the corresponding differences in the case of rigid spheroidal inclusions. From 5.6(b) we observe again that the differences are small for $c^{(2)} \leq 0.2$, but become increasingly more significant for higher values of the fiber volume fraction.

5.2 Nonlinear composites

In analogy to the previous section, we will apply the iterative procedure of subsection 4.2 to estimate the effective response of nonlinear composites. We will assume that the potentials $\psi^{(r)}$ are of the power-law form

$$\psi^{(r)}(\sigma_e) = \frac{\epsilon_0 \sigma_0^{(r)}}{n+1} \left(\frac{\sigma_e}{\sigma_0^{(r)}} \right)^{n+1}, \tag{5.19}$$

where $\sigma_e = \sqrt{3\boldsymbol{\sigma}_d : \boldsymbol{\sigma}_d/2}$ is the von Misses equivalent stress, n is the nonlinearity exponent (the inverse of the m = 1/n) and σ_0,ϵ_0 are reference strain and stress measures, respectively.

5.2.1 Rigid spherical inclusions

We focus our attention to a composite with the microstructure of Fig.5.1, consisting of rigid spherical inclusions (with stress potential equal to zero) reinforcing a power-law matrix phase. From (3.17) we have that the estimate for the effective shear modulus of the associated LCC

$$\tilde{\mu}_{[1]} = \mu_{[1]}^{(1)} \frac{2+3c}{2(1-c)} \tag{5.20}$$

Then, substituting (5.20) in expression (4.8), the second moment of the equivalent stress field in the matrix phase of the LCC is given by

$$\hat{\sigma}_{[1]}^{(1)} = \left(\frac{2}{2+3c} \right)^{\frac{1}{2}} \overline{\sigma}_{[1]}. \tag{5.21}$$

Next, using (5.21) in (4.6) we find that the normalized yield stress for the level-1 material is

$$\frac{\tilde{\sigma}_{[1]}^{IH}}{\sigma_0^{(1)}} = \frac{(1+\frac{3}{2}c)^{\frac{n+1}{2n}}}{(1-c)^{\frac{1}{n}}}. \tag{5.22}$$

Taking into account that the microstructure is identical in every scale of the composite and with heterogeneity contrast $\sigma_0^{(2)}/\tilde{\sigma}_{[i-1]}^{IH} = \infty$, follows immediately that

$$\frac{\tilde{\sigma}_{[i]}^{IH}}{\tilde{\sigma}_{[i-1]}^{IH}} = \frac{(1+\frac{3}{2}c)^{\frac{n+1}{2n}}}{(1-c)^{\frac{1}{n}}}. \tag{5.23}$$

Following Agoras and Ponte Castañeda [1] the normalized overal-effective yield stress may be written as

$$\frac{\tilde{\sigma}_{[N]}^{IH}}{\sigma_0} = \frac{\tilde{\sigma}_{[N]}^{IH}}{\tilde{\sigma}_{[N-1]}^{IH}} \cdots \frac{\tilde{\sigma}_{[2]}^{IH}}{\tilde{\sigma}_{[1]}^{IH}} \frac{\tilde{\sigma}_{[1]}^{IH}}{\sigma_0} \tag{5.24}$$

$$= \left(\frac{(1+\frac{3}{2}c)^{\frac{n+1}{2n}}}{(1-c)^{\frac{1}{n}}} \right)^N$$

$$= \frac{\left(\frac{5}{2} - \frac{3}{2}(1-c^{(2)})^{\frac{1}{N}} \right)^{\frac{N(n+1)}{2n}}}{\left(1-c^{(2)} \right)^{\frac{1}{n}}}, \tag{5.25}$$

and for the extreme case of an infinite number of steps this estimate reduces to

$$\frac{\tilde{\sigma}_{[\infty]}^{IH}}{\sigma_0} = \frac{1}{(1-c^{(2)})^{\frac{7+3n}{4n}}}. \tag{5.26}$$

In Fig. 5.7 results for the normalized effective yield-stress $\tilde{\sigma}_{0[N]}/\sigma_0$ are plotted for three specific values of the nonlinear exponent $n = 1, 3, 10$ of the matrix phase, as a function of the particle concentration $c^{(2)}$. More specifically, Fig. 5.7(a) presents $\tilde{\sigma}_{0[N]}/\sigma_0$ for $n = 3$ and $N = 1, 100$ and $N \to \infty$, and Fig.5.7(b) presents $\tilde{\sigma}_{0[N]}/\sigma_0$ for $n = 10$ and $N = 1, 100$ and $N \to \infty$, while Fig. 5.7(d) shows the differences of the incremental estimates from the corresponding variational estimates ($N = 1$) in percentage. From parts (a) and (b) we observe that the iterative estimate predicts a stronger material than the variational estimate, while from part (d) we see the difference is getting smaller as the nonlinearity of the matrix phase increases.

5.2.2 Porous composites

In this subsection we will specialize the incremental variational estimate to a porous, power-law material with the microstructure of Fig.5.1. First, we make use of (3.17) and (3.18) to calculate the effective shear and bulk modulus of the LCC associated with the level-1 porous material

$$\tilde{\mu}_{[1]} = \mu^{(1)} \frac{(1-c)}{1+\frac{2}{3}c} \qquad \text{and} \qquad \tilde{\kappa}_{[1]} = \mu^{(1)} \frac{4}{3} \frac{(1-c)}{c}. \tag{5.27}$$

From (3.21) follows that the effective response of the level-1 material is given by

$$\tilde{u}_{[1]}^{IH}(\overline{\boldsymbol{\sigma}}_{[1]}) = \sup_{\mu_{[1]}} \left\{ \frac{1}{6\tilde{\mu}_{[1]}} \overline{\sigma}_{e[1]}^2 + \frac{1}{2\tilde{\kappa}_{[1]}} \overline{\sigma}_{m[1]}^2 - (1-c) V_{[1]}(\mu_{[1]}) \right\}, \tag{5.28}$$

where the associated error function in this case is

$$V_{[1]}(\mu_{[1]}) = \sup_{\hat{\sigma}_{e[1]}} \left\{ \frac{1}{6\mu_{[1]}} \hat{\sigma}^2_{e[1]} - u_{[1]}(\hat{\sigma}_{e[1]}) \right\}. \tag{5.29}$$

From the optimality condition in equation (5.28) follows that

$$\hat{\sigma}_{e[1])} = \frac{1}{1-c} \sqrt{(1+\frac{2}{3}c)\overline{\sigma}^2_{e[1]} + (\frac{9}{4}c)\overline{\sigma}^2_{m[1]}}. \tag{5.30}$$

Then, by substituting the last results in (5.28), the expression for effective stress potential reduces to

$$\tilde{u}^{IH}_{(1)}(\overline{\boldsymbol{\sigma}}_{[1]}) = (1-c)\frac{\epsilon_0 \sigma_0}{n+1} \left\{ \frac{\left[(1+\frac{2}{3}c)\overline{\sigma}^2_{e[1]} + (\frac{9}{4}c)\overline{\sigma}^2_{m[1]} \right]^{\frac{1}{2}}}{(1-c)\sigma_0} \right\}^{n+1} \tag{5.31}$$

Next, we use (3.21) to estimate the effective stress-potential of the material in $\Omega_{[2]}$

$$\tilde{u}^{IH}_{[2]}(\overline{\boldsymbol{\sigma}}_{[2]}) = \sup_{\mu_{[2]},\, \kappa_{[2]}} \left\{ \frac{1}{6\tilde{\mu}_{[2]}} \overline{\sigma}^2_{e[2]} + \frac{1}{2\tilde{\kappa}_{[2]}} \overline{\sigma}^2_{m[2]} - (1-c) V_{[2]}(\mu_{[2]}, \kappa_{[2]}) \right\} \tag{5.32}$$

where the error function associated with the matrix phase of level-2 composite is

$$V_{[2]}(\mu_{[2]}, \kappa_{[2]}) = \sup_{\hat{\sigma}_{e[2]},\, \hat{\sigma}_{m[2]}} \left\{ \frac{1}{6\mu_{[2]}} \hat{\sigma}^2_{e[2]} + \frac{1}{2\kappa_{[2]}} \hat{\sigma}^2_{m[2]} - u_{[2]}(\hat{\sigma}_{e[2]}, \hat{\sigma}_{m[2]}) \right\} \tag{5.33}$$

and

$$u_{[2]}(\boldsymbol{\sigma}) \equiv \tilde{u}^{IH}_{[1]}(\boldsymbol{\sigma}) \tag{5.34}$$

Then, from the optimality conditions in (5.33) follows that

$$\mu_{[2]} = \frac{\hat{\sigma}_{e[2]}}{3\frac{\partial u_{[2]}(\hat{\sigma}_{e[2]}, \hat{\sigma}_{m[2])}}{\partial \hat{\sigma}_{e[2]}}} = \frac{(3a_{[1]})^{-1}}{A_{[1]}} \tag{5.35}$$

where

$$a_{[1]} = 1 + \frac{2}{3}c, \tag{5.36}$$

$$A_{[1]} = \left\{ \frac{\left[(1+\frac{2}{3}c)\hat{\sigma}^2_{e[2]} + (\frac{9}{4}c)\hat{\sigma}^2_{m[2]} \right]^{\frac{1}{2}}}{(1-c)\sigma_0} \right\}^{n} \frac{\epsilon_0}{\left[(1+\frac{2}{3}c)\hat{\sigma}^2_{e[2]} + (\frac{9}{4}c)\hat{\sigma}^2_{m[2]} \right]^{\frac{1}{2}}} \tag{5.37}$$

and

$$\kappa_{[2]} = \frac{\hat{\sigma}_{m[2]}}{\frac{\partial u_{[2]}(\hat{\sigma}_{e[2]}, \hat{\sigma}_{m[2])}}{\partial \hat{\sigma}_{m[2]}}} = \frac{b^{-1}_{[1]}}{A_{[1]}} \tag{5.38}$$

where

$$b_{[1]} = \frac{9}{4}c, \tag{5.39}$$

while from the optimality conditions in (5.32) we have that

$$\hat{\sigma}^2_{e[(2)]} = \frac{3}{(1-c)}\left[\frac{\partial(6\tilde{\mu}_{[2]})^{-1}}{\partial(2\mu_{[2]})^{-1}}\overline{\sigma}^2_{e[2]} + \frac{\partial(2\tilde{\kappa}_{[2]})^{-1}}{\partial(2\mu_{[2]})^{-1}}\overline{\sigma}^2_{m[2]}\right] \tag{5.40}$$

$$= \frac{\frac{9c\overline{\sigma}^2_{m[2]}}{4} + \frac{\left[27(3+2c)\kappa^2_{[2]}+48(3+2c)\kappa_{[2]}\mu_{[2]}+32(2+3c)\mu^2_{[2]}\right]\overline{\sigma}^2_{e[2]}}{(9\kappa_{[2]}+8\mu_{[2]})^2}}{(1-c)^2} \tag{5.41}$$

and

$$\hat{\sigma}^2_{m[2]} = \frac{2}{3(1-c)}\left[\frac{\partial(6\tilde{\mu}_{[2]})^{-1}}{\partial(3\kappa_{[2]})^{-1}}\overline{\sigma}^2_{e[2]} + \frac{\partial(2\tilde{\kappa}_{[2]})^{-1}}{\partial(3\kappa_{[2]})^{-1}}\overline{\sigma}^2_{m[2]}\right] \tag{5.42}$$

$$= \frac{\overline{\sigma}^2_{m[2]} + \frac{20c\kappa^2_{[2]}\overline{\sigma}^2_{e[2]}}{(9\kappa_{[2]}+8\mu_{[2]})^2}}{(1-c)^2} \tag{5.43}$$

By substituting (5.41) and (5.43) along with the corresponding expressions for $\mu_{[2]}$ and $\kappa_{[2]}$ in (5.32), the variational bound for the material in RVE $\Omega_{[2]}$, reduces to

$$\tilde{u}^{IH}_{[2]}(\overline{\boldsymbol{\sigma}}_{[2]}) = (1-c)^2\frac{\epsilon_0\sigma_0}{n+1}\left\{\frac{\left[a_{[2]}\overline{\sigma}^2_{e[2]} + b_{[2]}\overline{\sigma}^2_{m[2]}\right]^{\frac{1}{2}}}{(1-c)^2\sigma_0}\right\}^{n+1} \tag{5.44}$$

where

$$a_{[2]} = \frac{a_{[1]}\left[9a_{[1]}(3+2c) + 4b_{[1]}(2+3c)\right]}{27a_{[1]} + 8b_{[1]}}, \tag{5.45}$$

$$b_{[2]} = b_{[1]} + (\frac{9}{4}c)a_{[1]}. \tag{5.46}$$

The whole procedure is then repeated, until the desired volume fractions of the porous phase is reached. The overall effective-stress potential of the composite is given by

$$\tilde{u}^{VB}_{[N]}(\overline{\boldsymbol{\sigma}}) = (1-c)^N\frac{\epsilon_0\sigma_0}{n+1}\left\{\frac{\left[a_{[N]}\overline{\sigma}^2_{e[N]} + b_{[N]}\overline{\sigma}^2_{m[N]}\right]^{\frac{1}{2}}}{(1-c)^N\sigma_0}\right\}^{n+1}, \tag{5.47}$$

where

$$a_{[i]} = \frac{a_{[i-1]}\left[5(9a_{[i-1]} + 4b_{[i-1]}) - 6(3a_{[i-1]} + 2b_{[i-1]})(1-c^{(2)})^{\frac{1}{N}}\right]}{27a_{[i-1]} + 8b_{[i-1]}}, \tag{5.48}$$

$$b_{[i]} = b_{[i-1]} + \frac{9}{4}[1-(1-c^{(2)})^{\frac{1}{N}}]a_{[i-1]}, \tag{5.49}$$

$\overline{\sigma}_{e[i-1]} = \hat{\sigma}_{e[i]}$ and $\overline{\sigma}_{m[i-1]} = \hat{\sigma}_{m[i]}$, with $\overline{\sigma}_{e[N]} = \sqrt{3\overline{\boldsymbol{\sigma}}_d : \overline{\boldsymbol{\sigma}}_d/2}$ and $\overline{\sigma}_{m[N]} = \frac{1}{3}tr\overline{\boldsymbol{\sigma}}$.

Fig.5.8 compares yield surfaces for ideally plastic ($n \to \infty$) behavior for the matrix. In particular, 5.8(a) shows the results for $c^{(2)} = 0.1$ and $c^{(2)} = 0.2$ while in 5.8(b) the plots correspond to $c^{(2)} = 0.5$ and $c^{(2)} = 0.6$. For comparison purposes, we have also included the exact results from the composite sphere assemblage model (CSA) under pure hydrostatic loadings. From these results it is observed that IH predictions for the effective behavior of the porous material are softer than the corresponding CSA and the variational estimates (N=1), especially for high values of the porosity. Note, in particular, that the difference gets bigger for higher values of the stress triaxiality ($X_\sigma = \overline{\sigma}_m/\overline{\sigma}_e$), even for low porosity where differences are small in general.

5.2.3 Particle composites

We begin by considering a composite with the microstructure of Fig.5.1, made up from incompressible spherical inclusions (phase 2) embedded in an incompressible matrix material (phase 1). Both phases are assumed to be governed by power-law potentials of the form (5.19). Next, taking the limit $\kappa^{(1)} \to \infty$ and $\kappa^{(2)} \to \infty$ in (3.17), we find the following expression for the scalar effective modulus $\tilde{\mu}_{[1]}$ of the LCC associated with the material resulting from the first iteration

$$\tilde{\mu}_{[1]} = \frac{\mu_{[1]}^{(1)}\left[3(1-c)\mu_{[1]}^{(1)} + (2+3c)\mu_{[1]}^{(2)}\right]}{(3+2c)\mu_{[1]}^{(1)} + 2(1-c)\mu_{[1]}^{(2)}} \tag{5.50}$$

Substituting the above expression in the equations (4.15) we get

$$\frac{\hat{\sigma}_{[1]}^{(1)}}{\overline{\sigma}_{e[1]}} = \frac{\sqrt{6c(k_{[1]}-1)^2 + (3+2k_{[1]})^2}}{3+3c(k_{[1]}-1)+2k_{[1]}}, \quad \frac{\hat{\sigma}_{[1]}^{(2)}}{\overline{\sigma}_{e[1]}} = \frac{5k_{[1]}}{3+3c(k_{[1]}-1)+2k_{[1]}} \tag{5.51}$$

where we have made use of the notation $k_{[1]} = \mu_{[1]}^{(2)}/\mu_{[1]}^{(1)}$. Taking the ratio of the associated equations (4.14) for $\mu^{(r)}$ and making use of the above results we obtain the following nonlinear equation for $k_{[1]}$

$$\left(\frac{\sigma_0^{(2)}}{\sigma_0^{(1)}}\right)^n \left(\frac{6c(k_{[1]}-1)^2 + (3+2k_{[1]})^2}{25k_{[1]}^2}\right)^{\frac{n-1}{2}} = k_{[1]} \tag{5.52}$$

Then, substituting expressions (5.51) into (4.6), it follows that estimate for the normalized effective yield stress of the level-1 material is given by

$$\frac{\tilde{\sigma}_{0[1]}^{IH}}{\sigma_0} = \left\{(1-c)\left(\frac{\hat{\sigma}_{e[1]}^{(1)}}{\overline{\sigma}_{e[1]}}\right) + c\left(\frac{\hat{\sigma}_{e[1]}^{(2)}}{\overline{\sigma}_{e[1]}}\right)\left(\frac{\sigma_0^{(2)}}{\sigma_0^{(1)}}\right)^{-n}\right\}^{-\frac{1}{n}} \tag{5.53}$$

The whole procedure is then repeated successively, for each level $i = 2...N$ of the composite, with $\sigma_{0[i]}^{(1)} = \tilde{\sigma}_{[i-1]}^{IH}$. Finally, it turns out that the iterated effective yield stress is given by

$$\frac{\tilde{\sigma}^{IH}_{[N]}}{\sigma^{(1)}_0}=\frac{\left[3(1-c^{(2)})^{\frac{1}{N}}(1-k_{[N]})+5k_{[N]}\right]^{\frac{n+1}{n}}}{\left[5^{n+1}\left[1-(1-c^{(2)})^{\frac{1}{N}}\right]k^{n+1}_{[N]}t^{-n}+(1-c^{(2)})^{\frac{1}{N}}\left[5(3+2k^2_{[N]})-6(1-c^{(2)})^{\frac{1}{N}}(k_{[N]}-1)^2\right]\left(\frac{\tilde{\sigma}_{0[N-1]}}{\sigma^{(1)}_0}\right)^{-n}\right]^{\frac{1}{n}}},\tag{5.54}$$

where the variables $k_{[i]}$ are determined by solving the following set of nonlinear equation

$$\left(\frac{\sigma^{(2)}_0}{\tilde{\sigma}^{IH}_{[i-1]}}\right)^n\left(\frac{6\left[1-(1-c^{(2)})^{\frac{1}{N}}\right](k_{[i]}-1)^2+(3+2k_{[i]})^2}{25k^2_{[i]}}\right)^{\frac{n-1}{2}}=k_{[i]},\quad i=2,3,\ldots,N\tag{5.55}$$

In Fig.5.9 results for the normalized effective yield stress $\tilde{\sigma}_0/\sigma^{(1)}_0$ are plotted as a function of the nonlinearity for particle concentration $c^{(2)}=0.5$. As we see in Fig.5.9(a) for a composite with a particle to matrix contrast $t=\sigma^{(2)}_0/\sigma^{(1)}_0=0.2$ the IH results give slightly lower predictions for all values of the nonlinearity parameter $m=n^{-1}$. Fig.5.9(b) shows the percent difference of the IH estimate from the corresponding variational estimate for $t=0.2$. Fig.5.9(c) is the counterpart to Fig.5.9(a) in the particle reinforced case with $t=5$, where the IH estimate always remain above the variational estimate. The differences of the IH estimate from the corresponding variational estimate for $t=5$ are shown as percentages in Fig.5.9(d), where it is remarked that the maximum difference is observed for $m\approx 0.1$.

In Fig.5.10 results for $\tilde{\sigma}_0/\sigma^{(1)}_0$ of a particle-reinforced composite are shown as a function of the contrast $t=\sigma^{(2)}_0/\sigma^{(1)}_0$ for a fixed volume fraction $c^{(2)}$. For comparison purposes, we also include FEM results provided by Papadioti et.al [16]. The IH results are found to be above from both the VAR and FEM estimates for all values of t. In addition, it is observed that for $t<2.5$ the FEM results are a bit lower than the VAR. On the other hand for $t\geq 2.5$ the FEM results remain above the VAR results, and below the IH results, but always closer to the VAR estimates. We can see that both the VAR and IH estimates become constant as the contrast reaches a threshold contrast value. Specifically, for $c^{(2)}=0.4$ the threshold contrast values when using the VAR and IH methods are $r_{VAR}\approx 1.97$ and $r_{IH}\approx 3.34$, respectively.

5.2.4 Fiber composites

In this subsection we will focus on a nonlinear, fibrous composite which has the microstructure of Fig.5.1. The constitutive behaviors of the matrix and fibers are taken to be characterized by phase potentials of the power-law form (5.19). Following a similar procedure to that of the subsection 5.2.3 we obtain the following expression for the iterated effective in-plane yield stress of the associated composite

$$\frac{\tilde{\sigma}^{IH}_{[N]}}{\sigma^{(1)}_0}=\frac{\left[2k_{[N]}+(1-c^{(2)})^{\frac{1}{N}}(1-k_{[N]})\right]^{\frac{n+1}{n}}}{\left[(1-c^{(2)})^{\frac{1}{N}}\left[2(1+k^2_{[N]})-(1-c^{(2)})^{\frac{1}{N}}(1-k_{[N]})^2\right]^{\frac{n+1}{n}}\left(\frac{\tilde{\sigma}_{0[N-1]}}{\sigma^{(1)}_0}\right)^{-n}+2\left[1-(1-c^{(2)})^{\frac{1}{N}}\right]k^{n+1}_{[N]}t^{-n}\right]^{\frac{1}{n}}}, \tag{5.56}$$

where the variables $k_{[i]}$ are determined by solving the following set of nonlinear equation

$$\left(\frac{\sigma^{(2)}_0}{\tilde{\sigma}^{IH}_{[i-1]}}\right)^n\left(\frac{\left[1-(1-c^{(2)})^{\frac{1}{N}}\right](1-k_{[i]})^2+(1+k_{[i]})^2}{4k^2_{[i]}}\right)^{\frac{n-1}{2}}=k_{[i]},\quad i=2,3,\ldots,N \tag{5.57}$$

In addition, for the case of rigid fibers, the the corresponding effective in-plane yield stress is determined by following a the procedure of subsection 5.2.1

$$\frac{\tilde{\sigma}^{IH}_{[N]}}{\sigma^{(1)}_0}=\frac{\left(2-(1-c^{(2)})^{\frac{1}{N}}\right)^{\frac{N(n+1)}{2n}}}{\left(1-c^{(2)}\right)^{\frac{1}{n}}}, \tag{5.58}$$

In the limit as $N\to\infty$ the above result reduces to

$$\frac{\tilde{\sigma}^{IH}_{[\infty]}}{\sigma^{(1)}_0}=(1-c^{(2)})^{-\frac{3+n}{2n}} \tag{5.59}$$

Results of this subsection will presented and compared to results derived from the recently developed FOSO (Fully Optimized Second-Order) method for nonlinear homogenization (see for details J.Furer and Ponte Castañeda [7]). FOSO makes use of a more general LCC, leading to estimates that are more accurate than those resulting from earlier methodologies. We also include the Voigt-Reuss bounds for the effective behavior of the composite. The Voigt bound is an upper bound on the effective behavior, while the Reuss bound is a lower bound on the effective behavior. For our application the corresponding Voigt σ^V_0 and Reuss σ^R_0 bounds are given by

$$\left((1-c^{(2)})(\sigma^{(1)}_0)^{-n}+c^{(2)}(\sigma^{(2)}_0)^{-n}\right)^{-\frac{1}{n}}=\sigma^R_0\le\tilde{\sigma}_0\le\sigma^V_0=(1-c^{(2)})\sigma^{(1)}_0+c^{(2)}\sigma^{(2)}_0 \tag{5.60}$$

In one instance we will also present results from composite cylinder assemblage model (CCA). CCA model builds on an infinite number of cylinder sizes and is known to be an exact estimate for linear composites subject to some special loading conditions. However CCA model gives only an approximation for a nonlinear composites under in-plane loading.

In Fig.5.11 IH and VAR results for the normalized in-plane effective yield-stress are plotted as functions of m. From Fig.5.11(a) we observe that the IH estimates are stiffer than the corresponding variational estimates for all values of m. The deviation of the IH

estimate from the corresponding VAR estimate is shown in Fig.5.11(b) where the percent difference is plotted as a function of m. It is also observed that the difference decreases for decreasing values of m.

Fig.5.12 shows plots of the normalized yield stress for two values of the heterogeneity contrast $t = 0.2, 5$, as a function of the fiber concentration $c^{(2)}$. As we see in Fig.5.12(a), for a fiber-weakened composite the results from the variational estimates are in close agreement with those derived from FOSO and CCA in case of small nonlinearity. Moreover we notice that the IH estimate is (slightly) closer to the results from FOSO than the variational estimate. On the other hand, from Fig.5.12(b) we observe that for a fiber-reinforced material the VAR estimate is closer to FOSO for all values of m.

In Fig. 5.13 we plot the results for the normalized effective yield stress in the limit as $m \to 0$ as a function of the heterogeneity contrast $\sigma_0^{(2)}/\sigma_0^{(1)}$ for a fixed volume fraction $c_0^{(2)} = 0.2$. Fig. 5.13(a) shows plots for contrast $\sigma_0^{(2)}/\sigma_0^{(1)} \leq 1$ where we can see that the iterated variational bound tends to get closer to the estimates resulting from FOSO. Note that, since the fibers are weaker than the matrix, variational estimate constitutes an upper bound for the effective behavior of the composite. Exactly the opposite effect is observed when the composite is fiber-reinforced(Fig. 5.13(b)) where we notice that the difference gets bigger by iterating. Finally, it is relevant to remark that a common feature of the FOSO, VAR and IH methods is that after a value of heterogeneity contrast and above, depending on the volume fraction, predict that the inclusions act like rigid particles and the corresponding estimate becomes constant further on.

Figure 5.14 depicts the effective yield stress $\tilde{\sigma}_0$ normalized by $\sigma_0^{(1)}$ as a function of the fiber concentration $c^{(2)}$. Again, for a fiber-weakened material we observe that the IH estimate lies closer to FOSO estimate. In fact for large fiber concentrations $c^{(2)} > 0.5$ Fig.5.14(a) shows that the results from both methods are in very good agreement. In contrast, from Fig.5.14(b) we observe that the effective response predicted from the IH method for a fiber-reinforced composite is less close to FOSO than the corresponding prediction from the variational method.

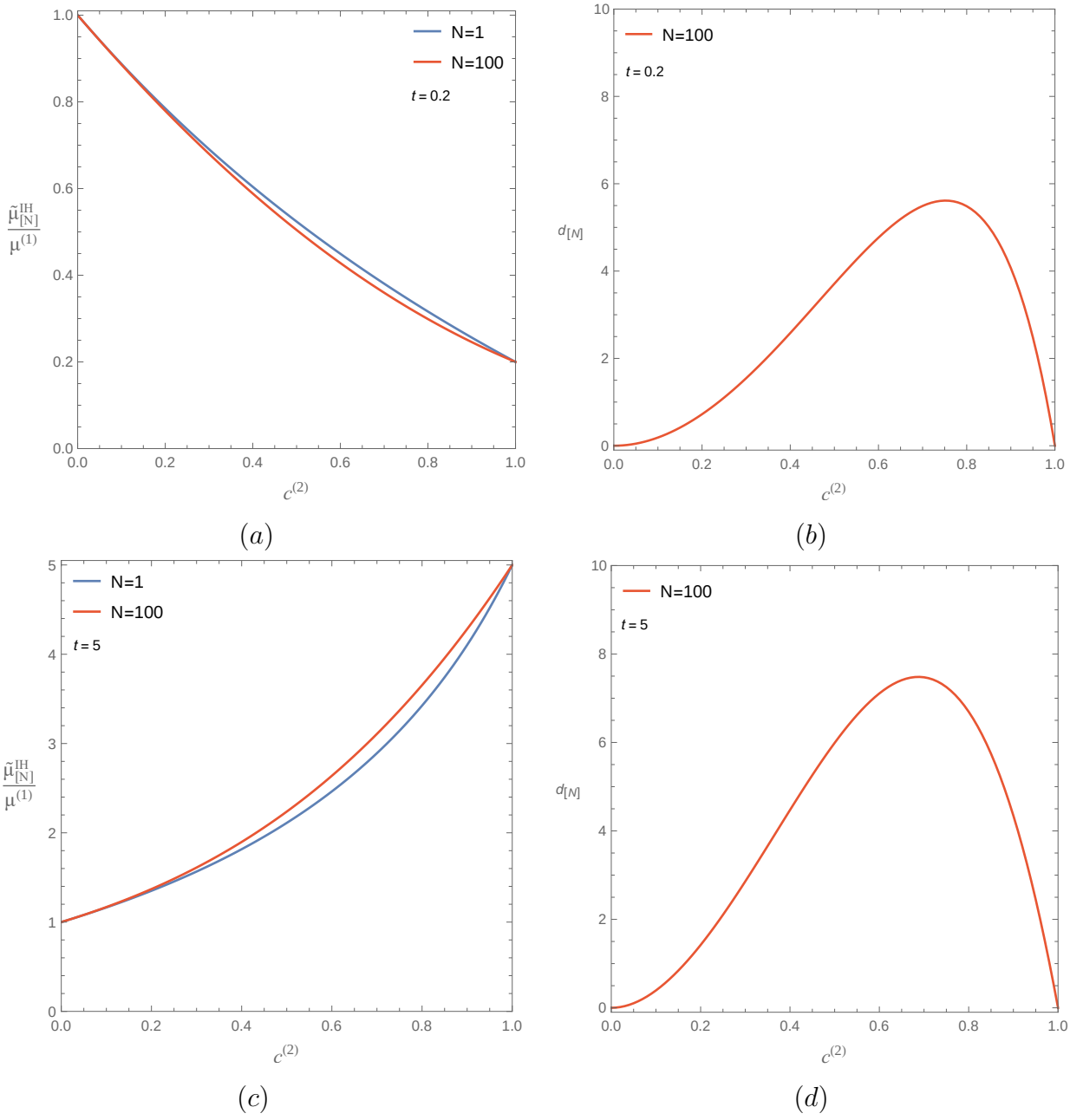

Figure 5.4: Results for the normalized effective shear modulus for a composite consisting of isotropic spherical particles embedded in an isotropic, incompressible, linear elastic matrix are plotted as a function of the concentration of particles $c^{(2)}$. (a) The normalized effective shear modulus as predicted by the IH and the HS (N=1) upper bound for a composite with heterogeneity contrast $t = 0.2$. (b) The percentage difference between the IH and the corresponding HS estimate for a composite with heterogeneity contrast $t = 0.2$. (c) The normalized effective shear modulus as predicted by the IH and the HS upper lower for a composite with initial heterogeneity contrast $t = 5$. (d) The percentage difference between the IH and the corresponding HS estimate for a composite with heterogeneity contrast $t = 5$.

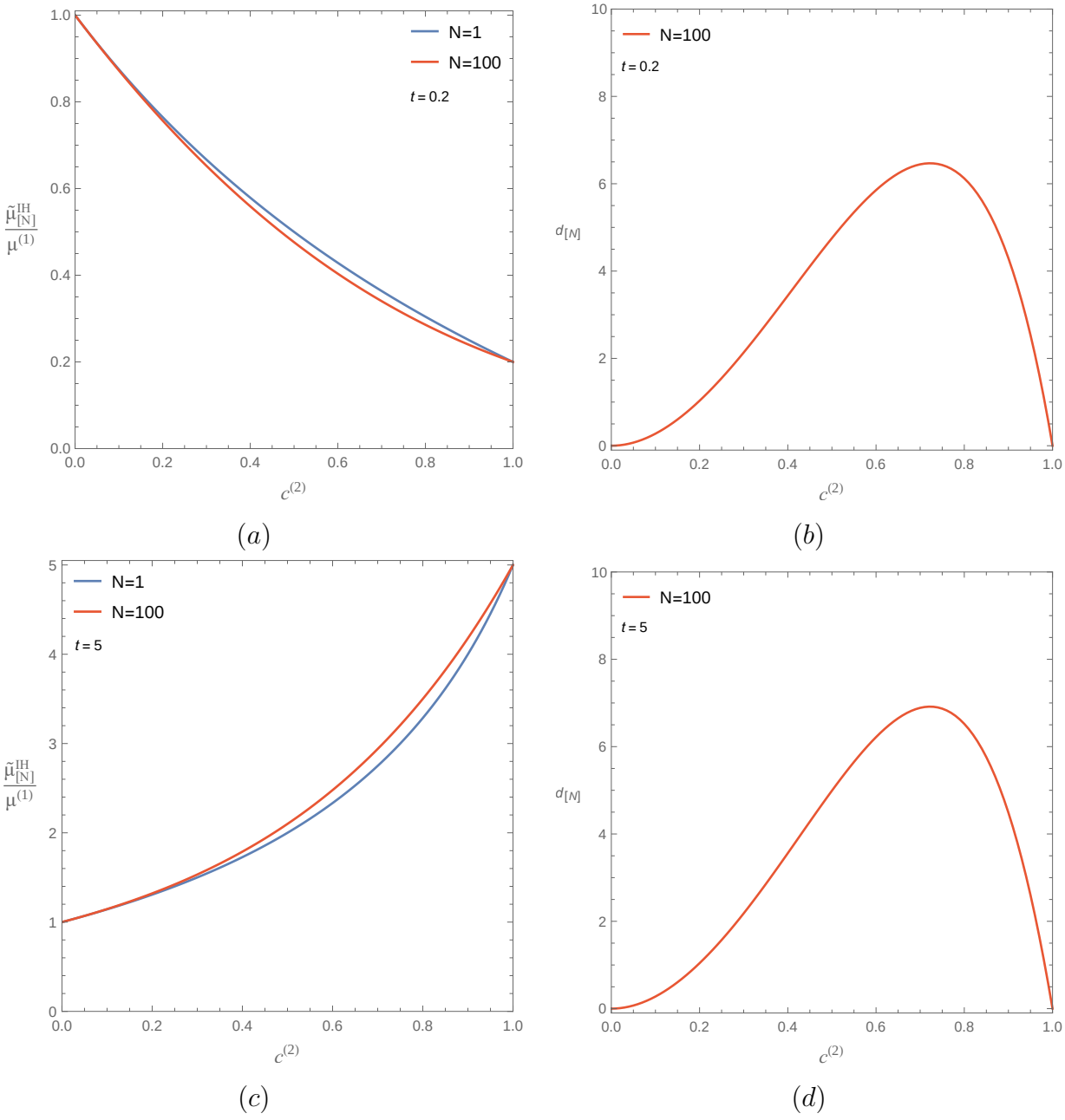

Figure 5.5: Results for the normalized effective in-plane shear modulus of an incompressible, linear elastic composite consisting of aligned fibers of circular cross-section embedded in an isotropic matrix material are plotted as a function of the concentration of particles $c^{(2)}$. (a) The normalized effective in-plane shear modulus as predicted by the IH and the HS (N=1) upper bound for a composite with heterogeneity contrast $t = 0.2$. (b) The percentage difference between the IH and the corresponding HS upper bound. (c) The normalized effective in-plane shear modulus as predicted by the IH and the HS lower lower for a composite with heterogeneity contrast $t = 5$. (d) The percentage difference between the IH and the corresponding HS lower bound

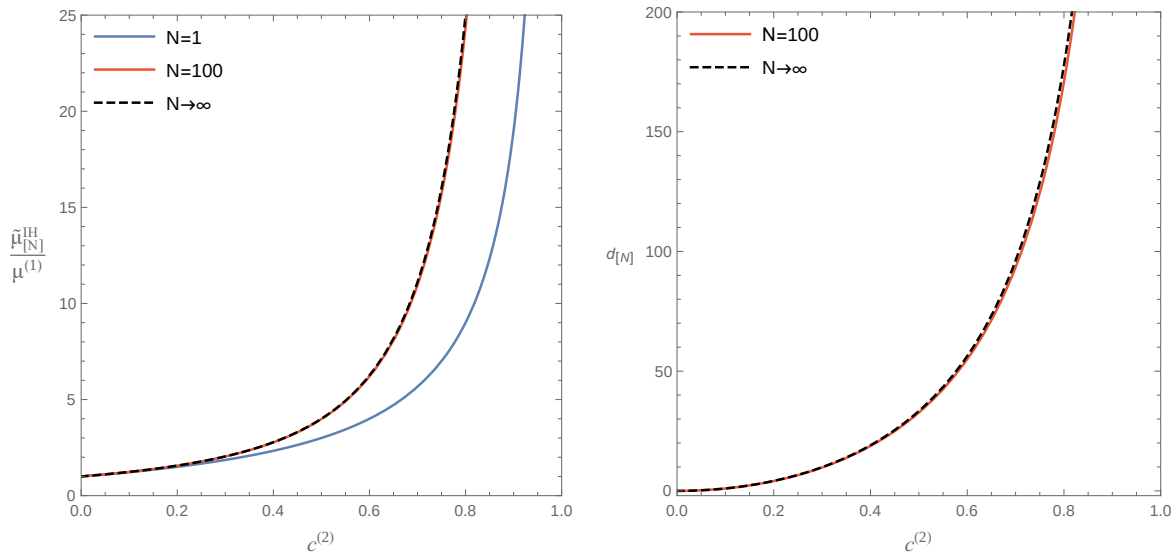

(a) (b)

Figure 5.6: IH estimates for the normalized effective in-plane shear modulus of a fiber-reinforced composite consisting of aligned rigid fibers embedded in an isotropic, incompressible, linear elastic matrix are plotted as a function of the fibers concentration. (a) The convergence of the IH estimate with increasing numbers (N) of increments, $N = 1, 100$ and $N \to \infty$ (b) The percentage difference $d_{[N]}$ between the IH estimate and the corresponding HS estimate for various values of N.

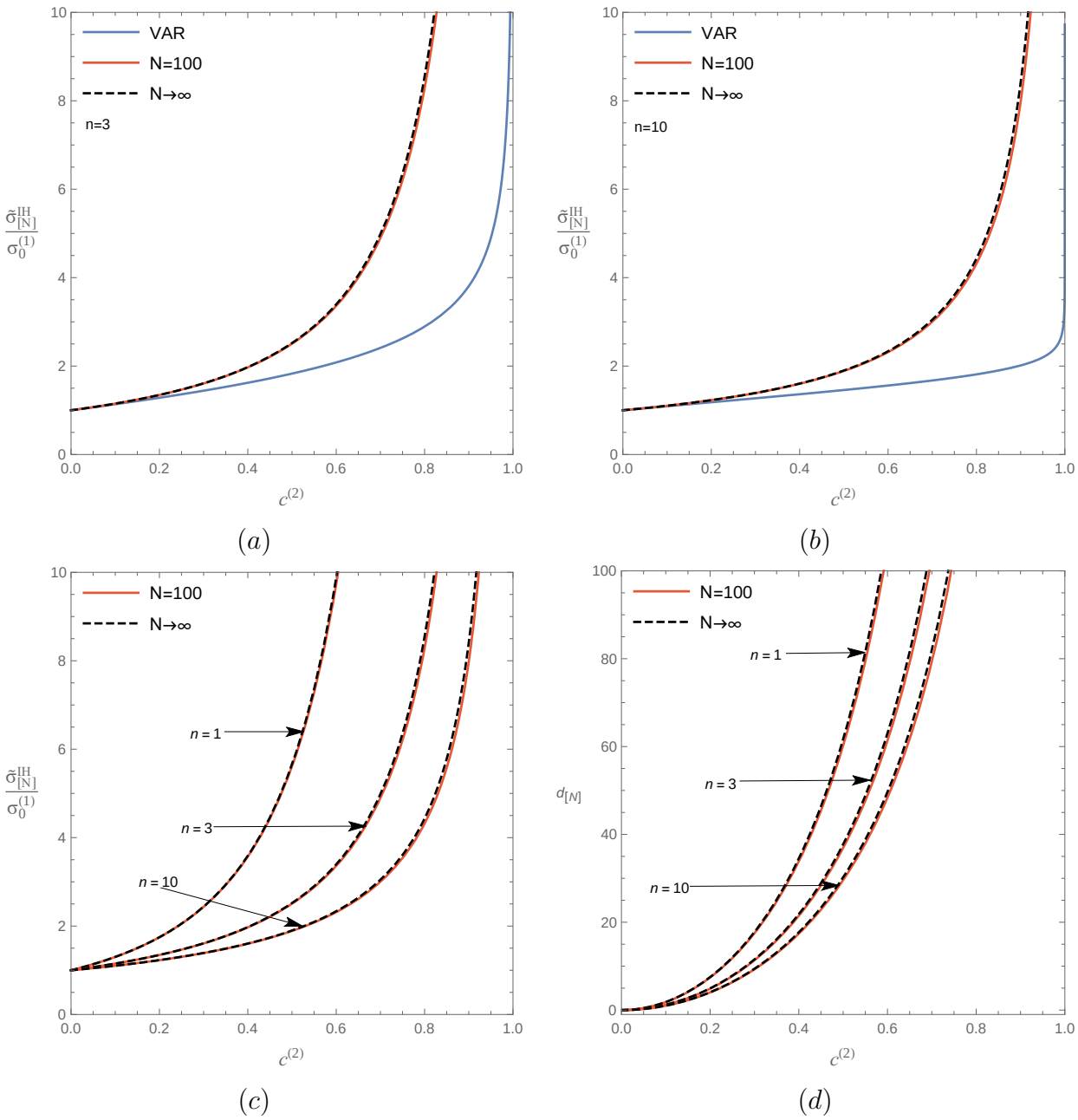

Figure 5.7: Comparison of IH and VAR estimates for the normalized effective yield-stress of a composite reinforced with rigid spherical particles embedded in a power-law matrix phase are plotted as a function of the concentration of particles $c^{(2)}$. Parts (a) and (b) shows $\tilde{\sigma}_0/\sigma_0^{(1)}$ for the cases $n = 3$ and $n = 10$, respectively.(c) The normalized effective yield-stress as predicted by the IH for $N = 100$ and $N \to \infty$, for three values of the nonlinear exponent $n = 1, 3, 10$. (d) The percent difference between the IH and the corresponding VAR estimates for $n = 1, 3, 10$.

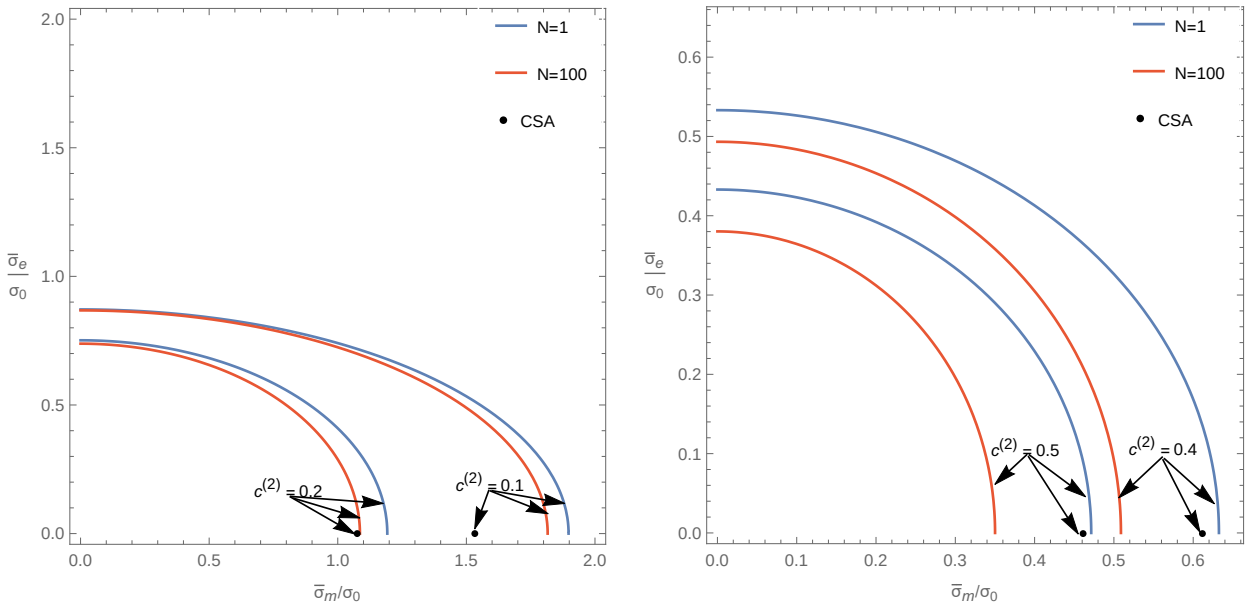

Figure 5.8: Plots of the effective yield surface obtained by the IH and VAR methods for isotropic porous materials consisting of spherical voids distributed in an ideally plastic matrix. (a) Plots for $c^{(2)} = 0.1, 0.2$ (b) Plots for $c^{(2)} = 0.4, 0.5$. CSA estimates are shown for comparison.

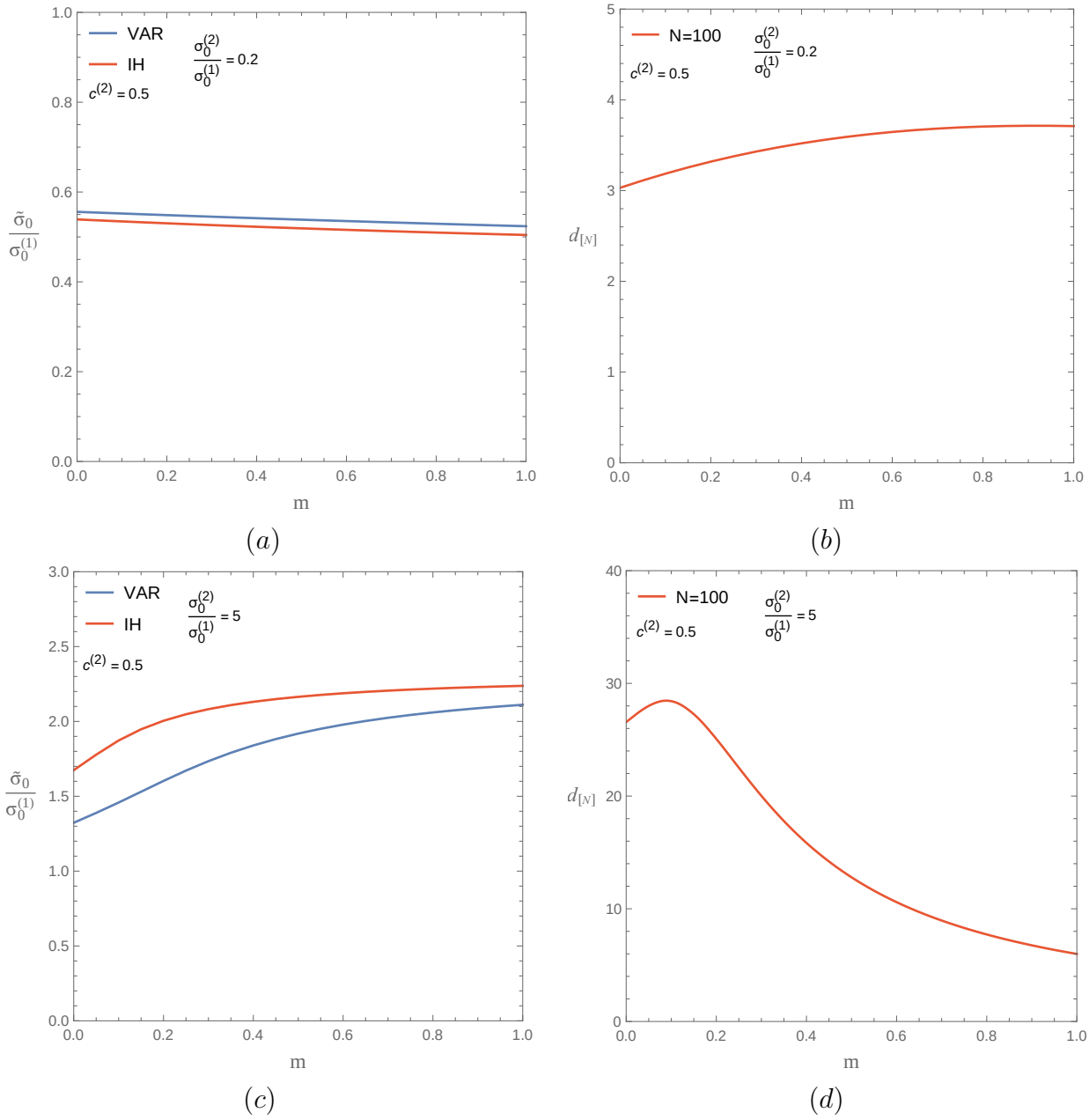

Figure 5.9: IH and VAR estimates for the normalized effective yield stress of a particulate composite consisting of spherical inclusion embedded in a power-law matrix, as a function of the nonlinearity m. The concentration of particles is $c^{(2)} = 0.5$. IH and variational estimates are shown in (a) for heterogeneity contrast $t = 0.2$, while the percent difference of the IH from the VAR estimate is shown in (b). Part (c) shows IH and variational estimates for particle to matrix contrast contrast $t = 5$ while the corresponding percent difference of the IH from the VAR estimate is shown in part (d)

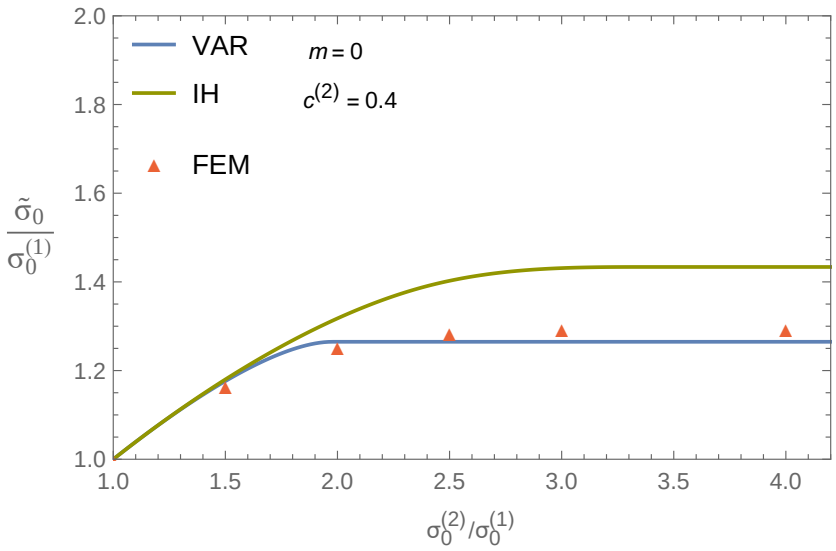

Figure 5.10: The normalized effective yield stress of a particle-reinforced composite for $c^{(2)} = 0.4$ and $m = 0$, as a function of the contrast $\sigma_0^{(2)}/\sigma_0^{(1)}$. Numerical results by Papadioti et.al [16] are shown for comparison.

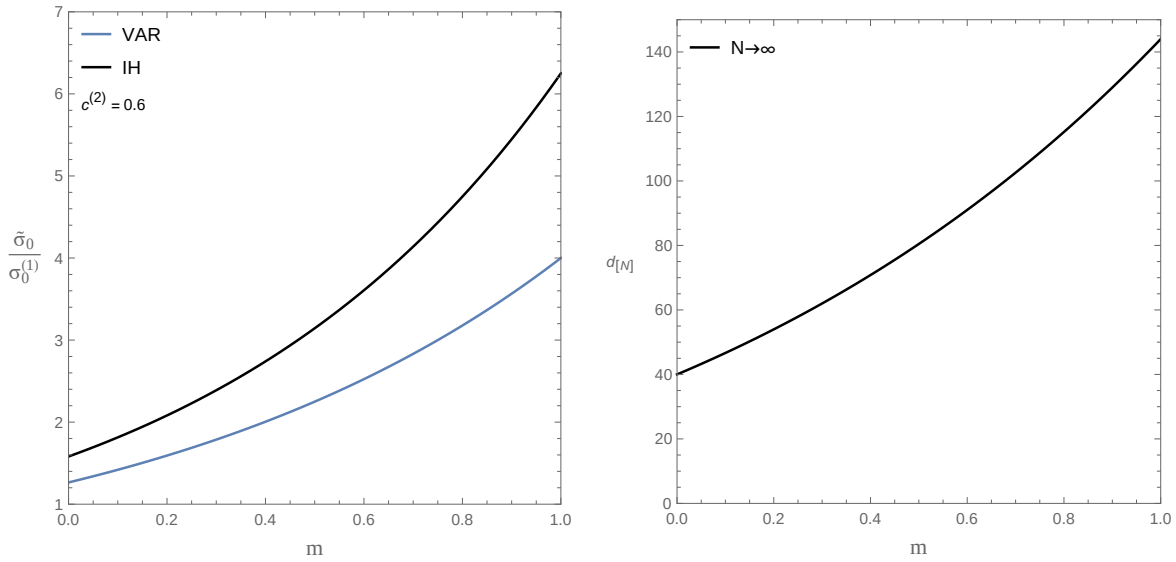

Figure 5.11: Comparison of the IH estimate and the corresponding variational estimate (VAR) for the normalized effective in-plane yield-stress $\tilde{\sigma}_0/\sigma_0^{(1)}$ of a rigidly fiber-reinforced composite with an incompressible matrix.(a) The VAR estimate and IH estimate for $N \to \infty$ are plotted as a function of m for a fixed volume fraction $c^{(2)} = 0.6$. (b) The precentage difference $d_{[N]}$ between the IH estimate and the corresponding VAR estimate.

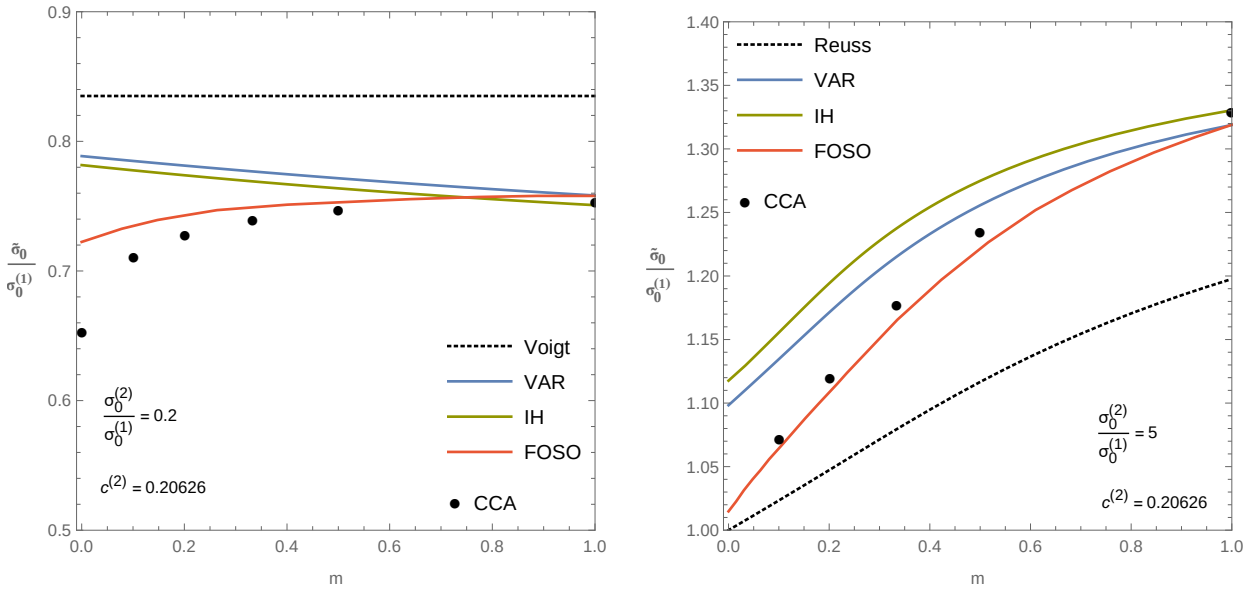

(a) (b)

Figure 5.12: The normalized effective in-plane yield stress $\tilde{\sigma}_0/\sigma_0^{(1)}$ of a fibrous composite with concentration $c^{(2)} = 0.20626$. Comparison of the IH estimate with the FOSO estimate, variational estimate (VAR) and the the Composite Cylinder Assemblage (CCA) for (a) a fiber-weakened composite with $t = 0.2$ and (b) a fiber-reinforced composite with $t = 5$, as a function of the nonlinearity m. The Voigt and Reuss bounds are also included in (a) and (b), respectively.

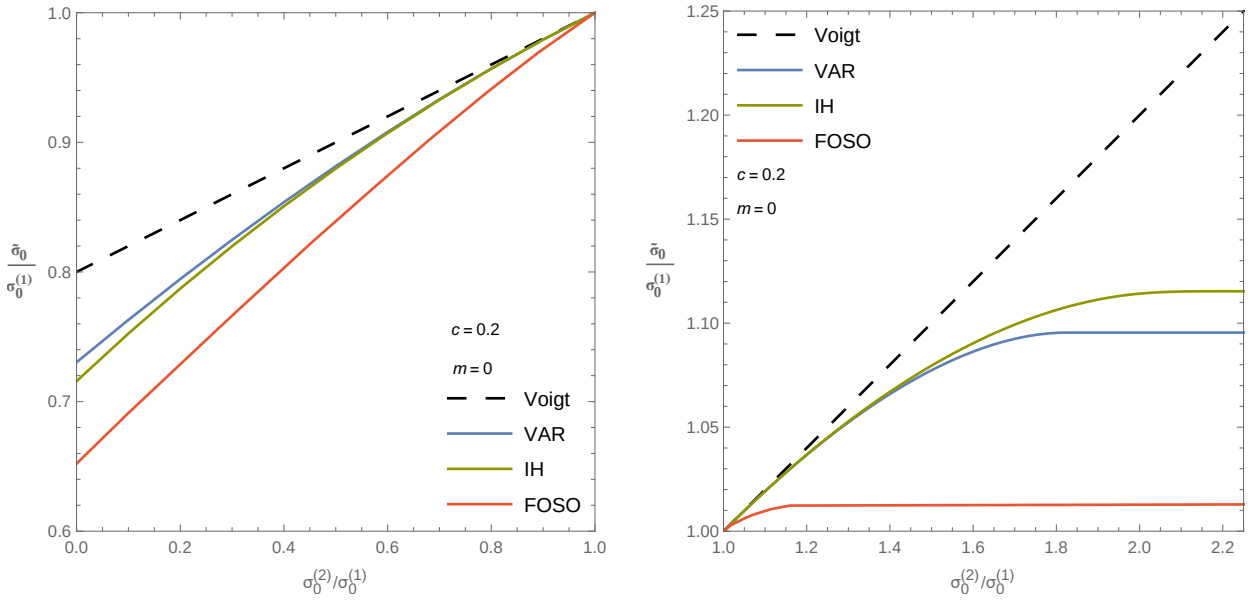

(a) (b)

Figure 5.13: The normalized effective in-plane yield stress $\tilde{\sigma}_0/\sigma_0^{(1)}$ of a fibrous composite with concentration $c^{(2)} = 0.2$. Comparison of the IH estimate with the FOSO estimate, the simple variational estimate (VAR) and the Voigt bound for (a) a fiber-weakened composite with $\sigma_0^{(2)}/\sigma_0^{(1)} < 1$ and (b) a fiber-reinforced composite with $\sigma_0^{(2)}/\sigma_0^{(1)} > 1$, as a function of the heterogeneity contrast $\sigma_0^{(2)}/\sigma_0^{(1)}$.

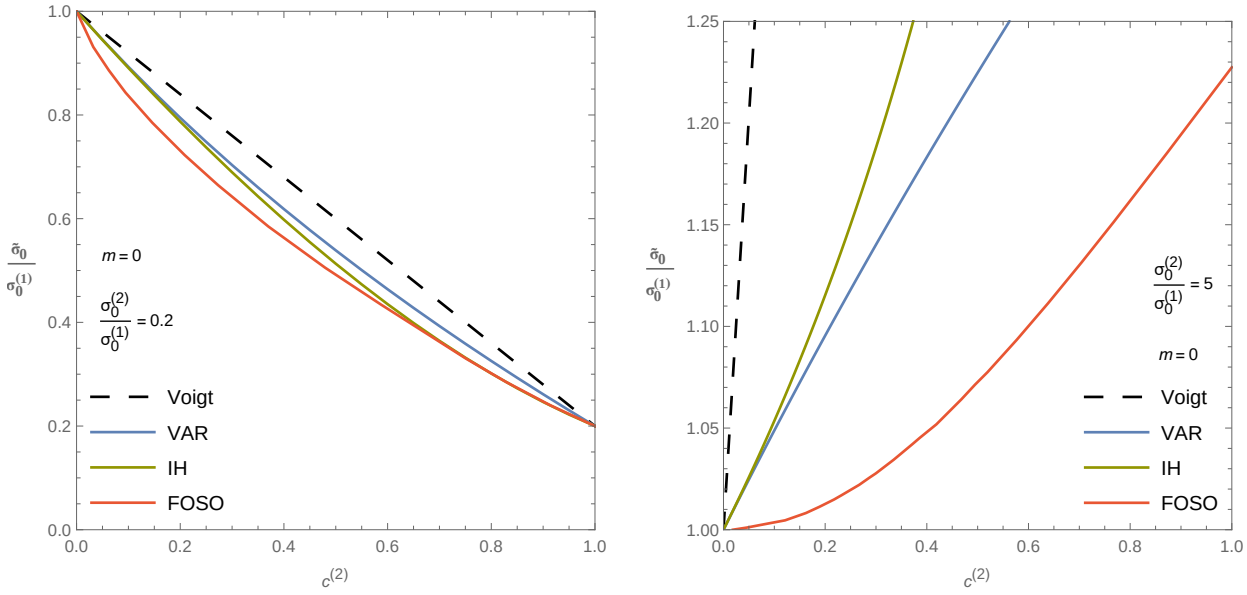

(a) (b)

Figure 5.14: The effective in-plane yield stress $\tilde{\sigma}_0$ of a fibrous composite normalized by $\sigma_0^{(1)}$. Comparison of the IH estimate with the FOSO estimate, variational estimate (VAR) and the Voigt bound for (a) a fiber-weakened composite with $\sigma_0^{(2)}/\sigma_0^{(1)} = 0.2$ and (b) a fiber-reinforced composite with $\sigma_0^{(2)}/\sigma_0^{(1)} = 5$, as a function of the fiber concentration $c^{(2)}$.

Chapter 6

Concluding remarks

In this thesis we have used a discretized version of the DS for estimating the effective behavior of particulate composites by means of iterated homogenization. At this point, it is relevant to recall that the PCW estimates [18] are sufficiently accurate for small and moderate concentrations of the inclusions, but on the other hand, for very high concentrations their accuracy deteriorates. Thus, the motivation behind the use of this homogenization procedure stems from the fact that allows us to homogenize every level of the resulting composite separately, where the added inclusions are in small concentration with respect to the previous effective medium.

For the applications of this incremental homogenization scheme we have considered four different cases in the context of linear elasticity and four more for nonlinear composites with power-law phases. The main conclusions are summarized in the following.

For a linear rigidly-reinforced material the differences between the IH estimate and the standard HS bound are significant especially at moderate to high concentrations. Furthermore, it was found that for an infinite number of increments the IH estimate reduces identically to the corresponding result from the DS, as it was expected. On the other hand, for small volume fractions of the particles the differences between the IH method and the HS bound are negligible. The next case we considered, was that of a linear porous medium. Again, the prediction of the iterated estimate is in agreement with the non-iterated for low values of porosity but we notice large differences for higher values of porosity, although smaller than the corresponding differences in the case of the rigidly reinforced composites. Moreover, it was found that the IH results for $N = 100$ match closely with the corresponding DS estimate (see Fig.5.8). For linear incompressible composites with heterogeneity contrast $t = 0,2$ and $t = 5$, described in detail in subsections 5.1.3 and 5.1.4, the differences between the iterated estimates and the HS bounds are limited in general, in contrast with the results from the previous two previous subsections. Finally, it is important to emphasize that in all cases considered the IH estimates obey the corresponding HS bounds, as they should.

For a nonlinear rigidly reinforced composite, the IH estimates are always stiffer than the corresponding variational estimates (VAR). In addition, it is observed that this difference decreases as the nonlinearity of the matrix increases (Fig.5.7(d)). On the other hand, for a nonlinear porous material the results predicted by the IH are found to be softer in comparison with the VAR results and the composite sphere assemblage (CSA)

predictions. It is also remarked that for high stress triaxialities ($X_\sigma = \overline{\sigma}_m/\overline{\sigma}_e$), differences between these methods become more apparent. For nonlinear incompressible composites with spherical particles we investigated the effective behavior in the ideally plastic limit. We saw that, for a particle-reinforced composite the IH estimates were, in general, always larger from the corresponding VAR estimates and the FEM predictions; moreover the FEM results were always closer to the VAR estimates. On the other hand, for a particle-weakened composite the IH estimates were always bellow the VAR results. Finally, in subsection 5.2.4 we applied the IH method to two-dimensional composites with microstructures consisting of statistically isotropic distributions of circular fibers in a matrix phase. The IH estimates were compared with the classical Voigt-Reuss bounds, the recently developed symmetric fully optimized second order method (FOSO) [7] and with estimates from the composite cylinders assemblage (CCA) model. It was found that for a fiber-weakened composite the IH results generally are closer to FOSO than the VAR estimate. In fact, Fig 5.14(a) shows that for high volume fraction $c^{(2)} > 0.5$ the IH results agree quite well with the corresponding results from FOSO. One the other hand, the exactly opposite effect is observed when the composite is fiber-reinforced.

Bibliography

[1] Agoras, M., Castañeda, P. P. (2011). Homogenization estimates for multi-scale nonlinear composites. European Journal of Mechanics-A/Solids, 30, 828-843.

[2] Agoras, M., Castañeda, P. P. (2013). Iterated linear comparison bounds for viscoplastic porous materials with "ellipsoidal" microstructures. Journal of the Mechanics and Physics of Solids, 61, 701-725.

[3] Bruggeman, V. D. (1935). Berechnung verschiedener physikalischer Konstanten von heterogenen Substanzen. I. Dielektrizitätskonstanten und Leitfähigkeiten der Mischkörper aus isotropen Substanzen. Annalen der physik, 416, 636-664.

[4] Bishop, J. F. W., Hill, R. (1951). XLVI. A theory of the plastic distortion of a polycrystalline aggregate under combined stresses. The London, Edinburgh, and Dublin Philosophical Magazine and Journal of Science, 42, 414-427.

[5] Bishop, J. F. W., Hill, R. (1951). CXXVIII. A theoretical derivation of the plastic properties of a polycrystalline face-centred metal. The London, Edinburgh, and Dublin Philosophical Magazine and Journal of Science, 42, 1298-1307.

[6] Eshelby, J. D. (1957). The determination of the elastic field of an ellipsoidal inclusion and related problems. *Proc. R. Soc. Lond. A* **241**, 376–396.

[7] Furer, J., Ponte Castañeda, P. (2017). A symmetric fully optimized second-order method for nonlinear homogenization: A symmetric fully optimized second-order method for nonlinear homogenization. ZAMM-Journal of Applied Mathematics and Mechanics/Zeitschrift für Angewandte Mathematik und Mechanik.

[8] Hashin, Z. (1962). The elastic moduli of heterogeneous materials. Journal of Applied Mechanics, 29, 143-150.

[9] Hashin, Z., Shtrikman, S. (1963). A variational approach to the theory of the elastic behaviour of multiphase materials. Journal of the Mechanics and Physics of Solids, 11, 127-140.

[10] Hershey, A. V. (1954). The elasticity of an isotropic aggregate of anisotropic cubic crystals. Journal of Applied mechanics-transactions of the ASME, 21, 236-240.

[11] Hill, R. (1964). Theory of mechanical properties of fibre-strengthened materials: I. Elastic behaviour. Journal of the Mechanics and Physics of Solids, 12, 199-212.

[12] Hill, R. (1963). Elastic properties of reinforced solids: some theoretical principles. Journal of the Mechanics and Physics of Solids, 11, 357-372.

[13] Michel, J. C., Suquet, P. (1992). The constitutive law of nonlinear viscous and porous materials. Journal of the Mechanics and Physics of Solids, 40, 783-812.

[14] Milton, G. W. (2002). The theory of composites. The Theory of Composites, by Graeme W. Milton, pp. 748. ISBN 0521781256. Cambridge, UK: Cambridge University Press, May 2002., 748.

[15] Norris, A. N. (1985). "A differential scheme for the effective moduli of composites." Mechanics of materials, 4.1, 1-16.

[16] Papadioti, I., Danas, K., Aravas, N. (2016). A methodology for the estimation of the effective yield function of isotropic composites. International Journal of Solids and Structures, 87, 120-138.

[17] Ponte Castañeda, P., Willis, J. R. (1988). On the overall properties of nonlinearly viscous composites. Proc. R. Soc. London A 416, 217–244.

[18] Ponte Castañeda, P., Willis, J. R. (1995). The effect of spatial distribution on the effective behavior of composite materials and cracked media. Journal of the Mechanics and Physics of Solids, 43(12), 1919-1951.

[19] Ponte Castañeda, P. (1991). The effective mechanical properties of nonlinear isotropic composites. Journal of the Mechanics and Physics of Solids, 39(1), 45-71.

[20] Ponte Castañeda, P. (1992). New variational principles in plasticity and their application to composite materials. Journal of the Mechanics and Physics of Solids, 40(8), 1757-1788.

[21] Ponte Castañeda, P. (1996). Exact second-order estimates for the effective mechanical properties of nonlinear composite materials. Journal of the Mechanics and Physics of Solids, 44(6), 827-862.

[22] Ponte Castañeda, P. Suquet, P., (1998). Nonlinear composites. Adv. Appl. Mech. 34, 171–302.

[23] Ponte Castañeda, P. (2002). Second-order homogenization estimates for nonlinear composites incorporating field fluctuations. I – Theory. J. Mech. Phys. Solids 50, 737–757.

[24] Ponte Castañeda, P. (2012). Bounds for nonlinear composites via iterated homogenization. J. Mech. Phys. Solids 60, 1583–1604.

[25] Suquet, P. (1987). Elements of homogenization for inelastic solid mechanics. In : Homogenization Techniques for Composite Media (E. Sanchez-Palencia and A. Zaoui, eds). Lecture Notes in Physics 272, Springer Verlag, Berlin, pp. 193–278.

[26] Talbot, D. R. S., Willis, J. R. (1985). Variational principles for inhomogeneous nonlinear media. IMA Journal of Applied Mathematics, 35, 39-54.

[27] Willis, J. R. (1977). Bounds and self-consistent estimates for the overall properties of anisotropic composites. Journal of the Mechanics and Physics of Solids, 25, 185-202.

[28] Willis, J. R. (1981). Variational and related methods for the overall properties of composites. Adv. Appl. Mech. 21, 1–78.

[29] Willis, J. R. (1989). The structure of overall constitutive relations for a class of nonlinear composites. IMA Journal of Applied Mathematics, 43, 231-242.

[30] Willis, J.R. (1991). On methods for bounding the overall properties of nonlinear composites. J. Mech. Phys. Solids 39, 73–86.

[31] Willis, J.R.,(1991). On methods for bounding the overall properties of nonlinear composites. J. Mech. Phys. Solids 39, 73–86.

[32] Willis, J.R. (2001). Mechanics of Composites. Lecture Notes, Ecole Polytechnique, pp.49–51.

[33] Zimmerman, R. W. (1991). Elastic moduli of a solid containing spherical inclusions. Mechanics of Materials, 12, 17-24.